Title

Morphometric and stable isotopic differentiation of Orbulina universa morphotypes from the Cariaco Basin, Venezuela

Authors

Marshall, Brittney J
Thunell, Robert C
Spero, Howard J
et al.

Publication Date

2015-10-01

DOI

10.1016/j.marmicro.2015.08.001

Peer reviewed

Marine Micropaleontology 120 (2015) 46–64

Contents lists available at ScienceDirect

Marine Micropaleontology

journal homepage: www.elsevier.com/locate/marmicro

Research paper

Morphometric and stable isotopic differentiation of *Orbulina universa* morphotypes from the Cariaco Basin, Venezuela

Brittney J. Marshall [a,*], Robert C. Thunell [a], Howard J. Spero [b], Michael J. Henehan [c], Laura Lorenzoni [d], Yrene Astor [e]

[a] Department of Earth and Ocean Sciences, University of South Carolina, Columbia, SC 29208, USA
[b] Department of Earth and Planetary Sciences, University of California, Davis, CA 95616, USA
[c] Department of Geology and Geophysics, Yale University, 210 Whitney Avenue, New Haven, CT 06511, USA
[d] College of Marine Science, University of South Florida, St. Petersburg, FL 33701, USA
[e] Estación de Investigaciones Marinas Isla Margarita, Fundación La Salle de Ciencias Naturales, Porlamar 6301, Venezuela

ARTICLE INFO

Article history:
Received 23 February 2015
Received in revised form 15 July 2015
Accepted 9 August 2015
Available online 24 August 2015

Keywords:
Planktonic foraminifera
Orbulina universa
Morphotypes
Cryptic species
Stable isotopes

ABSTRACT

Biometric characteristics of *Orbulina universa* (d'Orbigny) were used to differentiate two morphotypes present in sediment trap samples collected from the Cariaco Basin, Venezuela. Specifically, wall thickness and weight–area relationships were used to separate shells into thin (M_{thin}) and thick (M_{thick}) morphotypes. M_{thick} (mean thickness = 19–41 μm) comprises 75% of the total *O. universa* in these samples and has morphometric characteristics similar to that of the previously described Type I Caribbean genotype, whereas M_{thin} (mean thickness = 6–22 μm) is comparable to the Type III Mediterranean genotype. The flux of M_{thick} increases during periods of upwelling, whereas M_{thin} flux shows no systematic relationship with changing hydrographic regimes in the basin. The $\delta^{18}O$ and $\delta^{13}C$ of M_{thick} are on average 0.34‰ higher and 0.38‰ lower, respectively, than those of M_{thin}, suggesting that they calcify their final spherical chamber at different depths in the water column and/or differ in their vital effects on shell geochemistry. Additionally, the absolute offset in the stable isotopic compositions of the two morphotypes varies as a function of surface ocean stratification. During periods of upwelling, the $\delta^{18}O$ and $\delta^{13}C$ absolute offsets between M_{thin} and M_{thick} are on average −0.15 and 0.25‰, whereas average $\delta^{18}O$ and $\delta^{13}C$ absolute offsets between these two morphotypes increase to −0.54 and 0.41‰ during non-upwelling periods. We attribute the higher $\delta^{18}O$ and $\delta^{13}C$ offsets during non-upwelling periods to a difference in final chamber calcification depth and the combined effects of temperature ($\delta^{18}O$), $\delta^{13}C_{DIC}$ ($\delta^{13}C$), irradiance ($\delta^{13}C$) and $[CO_3^{2-}]$ ($\delta^{18}O$ and $\delta^{13}C$). These data provide field evidence that thin and thick morphotypes of *O. universa* likely experience different environmental conditions during the formation of their final chamber and, therefore, should not be combined in geochemical analyses for reconstructing past surface ocean conditions. Finally, we introduce a new proxy for reconstructing past surface ocean stratification changes via the use of M_{thin} and M_{thick} $\delta^{18}O$ and $\delta^{13}C$ offsets.

1. Introduction

1.1. Overview

The fossil shells of planktonic foraminifera serve as important sedimentary archives for studying past climatic and oceanographic conditions. However, proxy signals preserved in foraminiferal shells have been shown to vary significantly between species (Erez, 1978; Hemleben et al., 1989; Spero, 1998; Spero et al., 2003), with species identifications being strongly reliant on morphological concepts (Tendal, 1990). As a result of these interspecies differences, which are generally attributed to vital effects or ecological factors such as depth habitat and/or seasonal preferences, species-specific proxy calibrations are necessary in order to produce the most reliable estimates of past ocean conditions (Hemleben et al., 1989; Spero et al., 1997; Bijma et al., 1998; Bemis et al., 2002). Despite attempts to differentiate between morphologically defined species, the paleoceanographic community has long recognized the existence of morphotypes within species of planktonic foraminifera, often finding a large range in morphologies within a single population (Kennett, 1976; Deuser et al, 1981; Bé et al., 1983; Deuser, 1987; Deuser and Ross, 1989). A handful of studies report significant stable isotopic and trace element differences among different morphotypes of some species of planktonic foraminifera (Deuser et al., 1981; Healy-William et al., 1985; Deuser, 1987; Bijma et al., 1998; Wang, 2000; Steinke et al., 2005; Richey et al., 2012).

* Corresponding author at: Earth and Ocean Sciences, University of South Carolina, 701 Sumter Street, EWS 617, Columbia, SC 29208, USA.
E-mail address: Brittneyj.marshall@gmail.com (B.J. Marshall).

http://dx.doi.org/10.1016/j.marmicro.2015.08.001
0377-8398/

However, the significance of morphological variation was not apparent until the first genetic studies of foraminifera. These studies revealed that many morphologically defined species are complexes of cryptic genetic variants (Darling et al., 1996, 1997, 1999; de Vargas et al., 1997, 1999, 2003; Huber et al., 1997; Kucera and Darling, 2002; Darling and Wade, 2008). For example, fifty-four cryptic species have been identified among nine modern planktonic foraminiferal morphospecies commonly used for paleoceanographic reconstructions (Kucera and Darling, 2002; Darling and Wade, 2008; Morard et al., 2013). Several studies suggest that cryptic species can differ in their ecological preferences (Huber et al., 1997; Darling et al., 1999; de Vargas et al., 1999, 2003; Stewart et al., 2001; Kuroyanagi and Kawahata, 2004; Morard et al., 2009, 2013; Aurahs et al., 2011) and emphasize the importance of distinguishing between genotypes for paleoceanographic reconstructions (Kucera and Darling, 2002). Based on these findings, it is likely that a morphotype/genotype "lumping" approach for geochemical, morphometric and distribution analyses introduces a significant amount of noise into paleoclimate records. Thus, the ability to discriminate between these different genetic types within sediment samples may greatly enhance the usefulness of various planktonic foraminiferal proxies (Darling and Wade, 2008).

In some cases, taxonomic "lumping" may be easily revised within the framework of the morphospecies concept. For example, some genetically distinct variants of *Globigerinoides ruber* (Type IIa and Type Pink) can be differentiated easily based on differences in chamber morphometrics and pigmentation (Aurahs et al., 2011). Some cryptic species, however, are not distinguished from one another based on easily identifiable morphological differences (Knowlton, 1993). *Orbulina universa* (d'Orbigny), a species commonly used in climate proxy development (Spero and Williams, 1988; Sanyal et al., 1996; Spero et al., 1997; Bemis et al., 1998; Lea et al, 1999; Ren et al., 2012), has three known genetic variants — Caribbean (Type I), Sargasso (Type II) and Mediterranean (Type III; Darling et al., 1996, 1997; de Vargas et al., 1997, 1999; Morard et al., 2009). Several studies have mapped the geographic distribution of *O. universa* genotypes in the North and South Atlantic, Caribbean Sea, Western Pacific Ocean, Southern California Bight and Indian Ocean (Darling et al., 1997; de Vargas et al., 1997, 1999; Morard et al., 2009, 2013), and have linked their relative abundances to changes in sea surface chlorophyll concentrations (de Vargas et al., 1999). For example, plankton tow samples collected off Puerto Rico and Bermuda revealed the presence of both the Caribbean and Sargasso genotypes (de Vargas et al., 1997), which are defined as the oligotrophic and extreme oligotrophic genetic varieties of *O. universa*, respectively (de Vargas et al., 1999). *O. universa* collected from upwelling regions in the Atlantic and off the coast of California (Catalina Island) have been identified as the Mediterranean cryptic species, which is considered to be the eutrophic variant of *O. universa* (de Vargas et al., 1999). Morard et al. (2009) further documented the presence of all three cryptic species at a Caribbean sampling site (C-Marz 5; 14°01′N, 54°91′W), only 1200 km NW of the Cariaco Basin sediment trap mooring.

These three cryptic species of *O. universa* are morphologically very similar, but subtle differences in pore space distribution and shell wall thickness have been used to distinguish them using a scanning electron microscope (SEM; Morard et al., 2009). However, this is a time consuming process and the identification of the cryptic species in this way does not always permit subsequent geochemical analysis of the shells due to sample processing for SEM analysis. The current study presents a framework for the identification of morphotypes and potentially cryptic species of *O. universa*. Our results suggest that there are currently two morphotypes of *O. universa* characterized by thin and thick shell walls (M_{thin} and M_{thick}) present in the Cariaco Basin that can be separated on the basis of shell morphology. We also present carbon and oxygen isotope data in an attempt to better constrain the ecological preferences and final spherical chamber calcification depths of the two morphotypes.

1.2. Orbulina universa: life cycle, habitat preferences and morphometric variability

Early studies of the habitat preferences and morphological characteristics of *O. universa* treated its morphotypes as ecophenotypic variants, all belonging to the same genetic species but exhibiting phenotypic variation under different environmental conditions (Bé et al., 1973; Hecht et al., 1976; Colombo and Cita, 1980). These studies defined *O. universa* as a temperate–subtropical–tropical species with a preference for dwelling within the photic zone between the surface-mixed layer and shallow thermocline. The temperature ranges reported for *O. universa* differ regionally, but generally fall between 9 and 30 °C (Bradshaw, 1959; Tolderlund and Bé, 1971; Bouvier-Soumagnac and Duplessy, 1985; Sautter and Thunell, 1991; Darling and Wade, 2008).

During the early portion of its ~1 month life cycle (Hemleben and Bijma, 1994), *O. universa* has a multi-chambered trochospiral form, ornamented with calcite spines that serve as a home for a cloud of photosynthetic dinoflagellate symbionts. During the last 2–9 days of its life cycle, *O. universa* precipitates a large, spherical chamber that comprises 90–95% of its total calcite and thickens continuously until gametogenesis (Spero, 1988; Spero et al., 2015). The sphere is the final chamber addition phase of this species. During gametogenesis, *O. universa* sheds its spines and adds a thin veneer of calcite that contributes ~4–20% to the final shell calcite prior to the release of its gametes (Hamilton et al., 2008). Small and large pores on the final chamber serve as pathways for gas exchange and food and symbiont movement into and out of the cell protoplasm, respectively (Bé et al., 1980; Spero, 1987, 1988). Pore distribution is established at the time of initial sphere formation (Spero, 1988), and is believed to be distinctly different among the genetic varieties of *O. universa* (Morard et al., 2009).

Size variations in the final spherical chamber of *O. universa* have been linked to changes in calcification temperature (Schmidt et al., 2004; Lombard et al., 2009), whereas thickness variations have been associated with changes in the carbonate ion concentration ($[CO_3^{2-}]$) and variations in water column irradiance (related to symbiont photosynthesis; Lea et al., 1995; Lombard et al., 2010; Spero et al., 2015). Porosity variations in *O. universa* specimens have been attributed to changes in oxygen concentrations, such that porosity increases as oxygen concentrations decrease (Colombo and Cita, 1980). However, since *O. universa* spends its life cycle within the photic zone, where dissolved O_2 is saturated or oversaturated, changes in oxygen concentration are an unlikely contributor to porosity variations. Additionally, the discovery of porosity and thickness differences between cryptic species of *O. universa* complicates these earlier ecophenotypic concepts (Morard et al., 2009).

Deuser et al. (1981) and Deuser (1987) were the first to suggest a difference in calcification depths for morphotypic variants of *O. universa* based on sediment trap material collected from the Sargasso Sea (32°54′N, 64°15′W). These studies report the presence of thin (5–10 μm) and thick (up to 30 μm) morphotypes of *O. universa* and find that the thick walled variety secretes shells that have up to 0.5‰ higher $\delta^{18}O$ values than the thin-walled variety (Deuser et al., 1981). The thin morphotype comprised 65–80% of the *O. universa* collected at this location and was present year-round, though in higher abundances during periods of increased stratification. The thick-walled variety was far less abundant (20–35%), and is only present in this region of the North Atlantic during the summer when the mixed layer is deep. Based on oxygen isotopic compositions of pooled sediment trap shells and depth-stratified plankton tow samples, Deuser et al. (1981) concluded that the thinner of the two morphotypes calcified at depths between 25 and 50 m, while the thicker morphotype calcified in deeper water. The thickness variations between the two morphotypes were ultimately attributed to the presence or absence of gametogenic calcite, though later studies suggest that the *O. universa* morphotypes from these studies may represent different cryptic species (Hamilton et al., 2008). Deuser (1987) also report that the differences between the

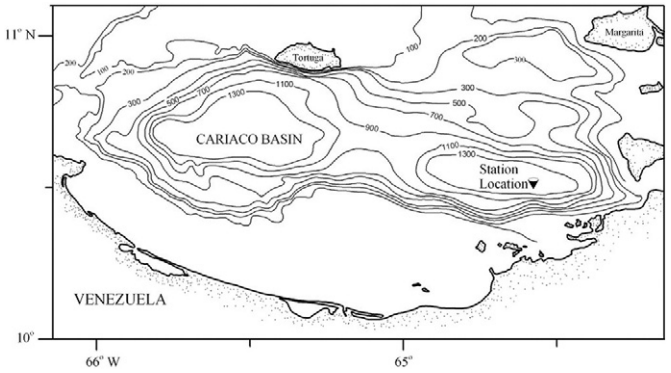

Fig. 1. Bathymetric map of the Cariaco Basin showing the location of the sediment trap mooring (10°30′N and 65°31′W).

oxygen isotopic compositions of the thick and thin varieties of *O. universa* is minimal during periods when the mixed layer is deep and increases rapidly as a more stratified water column is established.

1.3. The CARIACO Ocean Time Series

The Cariaco Basin is located on the continental shelf of northern Venezuela (Fig. 1). Because of the shallow sills (~130 m) surrounding the basin, the deep waters are not well ventilated. This restricted nature of the basin, combined with seasonally high productivity, results in anoxic waters below ~250 m. The CARIACO Ocean Time Series was established in November 1995 and provides a repository of biweekly sediment trap samples collected at discrete depths throughout the water column (10°30′N and 65°31′W; 150, 230, 410, 800 and 1200 m). Monthly hydrographic data are also available for comparison with sediment trap data. These samples have been used to assess and further calibrate a variety of paleoceanographic proxies (Goni et al., 2004; Marshall et al., 2013; Turich et al., 2013; Wejnert et al., 2013).

The physical and chemical characteristics of Cariaco Basin surface waters vary seasonally in response to the migration of the Intertropical Convergence Zone (ITCZ). When the ITCZ is in its most northerly position (August–October), temperatures and pH are high and salinity and nutrient concentrations are low in the surface waters. As the ITCZ shifts further south during boreal winter and early spring, the basin is exposed to strong easterly trade winds that result in Ekman-induced upwelling (Astor et al., 2013). Enhanced upwelling during the winter and spring results in lower temperatures and pH and higher salinities and nutrient concentrations in the surface waters. Fig. 2 illustrates seasonal changes in surface ocean temperature throughout the study period (July 2005–January, 2008) due to changes in upwelling intensity in the basin. The dynamic nature of the basin allows us to observe a wide range of hydrographic conditions and assess their impact on the planktonic foraminifera that calcify within the basin.

2. Methods

2.1. Sediment trap and water property collections

We use biweekly sediment trap samples from the trap moored at 410 m depth and collected between August 2005 and July 2008. The foraminifera were separated from a quarter split of each sample cup using the settling method presented in Bé (1959). The samples were then wet sieved (>125 μm) and washed prior to being examined under a stereo binocular microscope. All *O. universa* specimens within the quarter split were wet picked and counted. The number of specimens in each sample ranged from 13 to 56, with an average of 33. The fluxes of each morphotype were calculated by:

$$\text{Flux}\,(\text{n/m/day}) = 4\text{n}/(0.5\ \text{m})/\text{days} \quad (1)$$

where n is the number of specimens of a given morphotype in a quarter split of each sample population, 0.5 m is the cross-sectional area of the sediment trap and days is the duration of the collection period (7–14 days; Tedesco and Thunell, 2003).

Monthly temperature, salinity, oxygen, pH, chlorophyll and nutrient concentrations measured at the sediment trap mooring location were compared to the morphotype fluxes, oxygen isotope-derived calcification temperatures, and morphometric characteristics of the *O. universa* specimens. Irradiance measurements for the upper 75 m of the water column were also available for select samples throughout the study period (Lorenzoni et al., 2011). Temperature and salinity measurements were used to establish mean calcification depths of the final sphere for each morphotype (this procedure is described in Section 2.5). A comprehensive listing of the monthly hydrographic data for the entire Cariaco Basin time series can be found at http://www.imars.usf.edu/CAR. Because the vast majority (90–95%) of *O. universa* sphere calcite is produced at the end of its life cycle (Spero et al., 2015), and considering a 1 to 2-day settling period to reach the trap depth of 410 m (sinking speed = 300 m/day; Takahashi and Bé, 1984), the foraminifera collected in the biweekly sediment traps could have calcified from 8 days prior to 11 days after the time the trap opened for collection. To account for this, we paired the sediment trap samples with hydrographic data that fell closest to or within this time range when possible. The dates for the beginning of each sediment trap collection period, the paired date of hydrographic data collection, and the values for the surface ocean

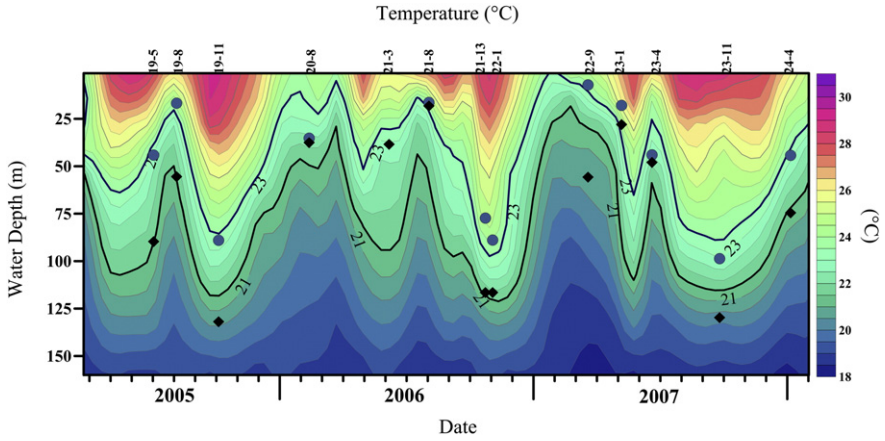

Fig. 2. Temperature record for the upper 130 m throughout the study period (July 2005–January 2008). Estimated calcification depths of *O. universa* M_{thin} (blue circles) and M_{thick} (black diamonds) are plotted for the study period. The bolded numbers along the upper x-axis indicate the sample IDs of the plotted data.

Table 1
Morphotype fluxes and surface hydrographic parameters (0–100 m average). Gray shaded samples correspond with upwelling periods.

Sample ID	Trap date	Hydro date	Date difference	M_{thin} (n)	M_{thick} (n)	Total (n)	Flux M_{thin} (n/m/day)	Flux M_{thick} (n/m/day)	Combined flux (n/m/day)	Temp (°C)	Salinity	$[PO_4^{3-}]$ (μmol/kg)	Chl (ng/L)	O_2 (μmol/kg)	pH
19_5	7/13/2005	7/12/2005	−1	5	13	18	3	7	10	24.13	36.89	0.18	210	169	8.01
19_8	8/24/2005	8/10/2005	−14	8	35	43	5	20	25	22.84	36.89	0.25	176	160	7.99
19_11	10/5/2005	10/5/2005	0	9	17	26	5	10	15	26.92	36.70	0.10	206	183	8.06
20_7*	2/7/2006	2/7/2006	0	12	38	50	7	22	29	22.14	36.81	0.26	1401	173	7.98
20_8	2/21/2006	2/7/2006	−14	13	43	56	7	25	32	22.14	36.81	0.26	1401	173	7.98
21_3	6/14/2006	6/6/2006	−8	0	21	21	0	12	12	23.65	36.88	0.09	163	167	8.00
21_8	8/23/2006	8/3/2006	−20	14	33	47	8	19	27	22.61	36.77	0.25	291	149	7.96
21_13	11/1/2006	10/10/2006	−22	5	13	18	3	7	10	24.24	36.68	0.19	366	175	8.01
22_1	11/8/2006	11/2/2006	−6	10	3	13	6	2	7	26.73	36.44	0.11	126	182	8.06
22_7*	1/31/2007	2/6/2007	6	13	23	36	7	13	21	21.48	36.71	0.38	1761	156	7.95
22_9	2/28/2007	3/6/2007	6	11	22	35	6	13	19	21.40	36.69	0.38	509	150	7.94
23_1	5/16/2007	5/8/2007	−8	4	34	38	2	19	22	23.00	36.81	0.28	192	155	7.95
23_4	6/27/2007	7/3/2007	6	5	28	33	3	16	19	23.01	36.80	0.29	312	152	7.96
23_11	10/3/2007	10/9/2007	6	18	20	38	10	11	22	25.99	36.63	0.10	215	179	8.05
24_4	1/8/2008	1/10/2008	2	8	11	19	5	6	11	25.44	36.78	0.12	312	189	8.04
Mean			−4	9	24	33	5	13	19	23.71	36.75	0.22	509	168	8.00

hydrographic measurements (upper 100 m average) are reported in Table 1.

We use the coastal upwelling index (M; m^3/s), estimated based on the cross-shore Ekman transport per 100 m of coastline, to identify periods of upwelling and non-upwelling throughout the study period (Astor et al., 2013):

$$M = \tau_x / f \tag{2}$$

where M is the meridional Ekman transport, τ_x is the zonal wind stress derived from nearby meteorological stations and f is the Coriolis parameter. The monthly upwelling index anomaly is then calculated by dividing M by the average M for the study period of January 1996–November 2011, with a negative anomaly representing periods of enhanced upwelling. Here, we define an upwelling period as an upwelling index anomaly ≤0.

2.2. Foraminiferal morphometric calculations

Individual foraminifera (n = 13–56 per sample) were weighed on a high-precision Mettler Toledo microbalance (±0.43 μg) and photographed using an inverted microscope equipped with a Canon Rebel XSI. The photographs were analyzed using the microscopic imaging program Macnification 2.0 for diameter and silhouette area analysis. Calibrations for the silhouette area and diameter measurements were performed using a microscale image taken at the same magnification as the foraminiferal images (50×). The area densities (ρ_A) of individual *O. universa* were calculated using the methods presented in Marshall et al. (2013), where

$$\rho_A \left(\mu g/\mu m^2\right) = \text{weight/silhouette area}. \tag{3}$$

The mean area densities (ρ_A) for each sediment trap sample were calculated by averaging the ρ_A of all *O. universa* specimens in a given sample. A total of 494 *O. universa* specimens were measured for weight, silhouette area, diameter, and area density in this study.

2.3. Orbulina universa morphotype distinction

The area densities of individuals were used to create groupings of *O. universa* morphotypes for each of the 15 sediment trap samples. Examples of this method applied to two of the samples (20-8 and 23-4) are shown in Fig. 3A and B. The area densities for all samples are shown in Fig. 3C. As the groupings were created, the weights and areas of each group exhibited distinct positive linear relationships (Fig. 3D–E), providing a secondary means of distinguishing *O. universa* morphotypes. The morphotype-specific weight–area relationships for all samples are shown in Fig. 3F. All but one sample exhibited two distinct morphotype groupings, a thin morphotype (M_{thin}) and a relatively thick morphotype (M_{thick}). For the sample containing a single morphotype (21-3), we compare the mean weight, area and area density to the ranges exhibited by each morphotype and are able to easily classify this group as M_{thick} (Fig. 3C and F).

2.4. SEM analyses

O. universa individuals from two of the samples (20-7 and 22-7; n = 42) used in the morphometric analysis were also examined on a Tescan Vega 3 SBU variable pressure scanning electron microscope (SEM). The *O. universa* shells were gently broken, attached to carbon tape and gold sputter-coated to prevent charging of the specimen during imaging. Porosity measurements were made on these specimens by gathering images normal to the inner shell wall in order to minimize optical distortion of the pores (Bé et al., 1973; Spero, 1988). The outer edges of each individual were used to measure shell thickness. Images were uploaded into the microscopic imaging program Macnification

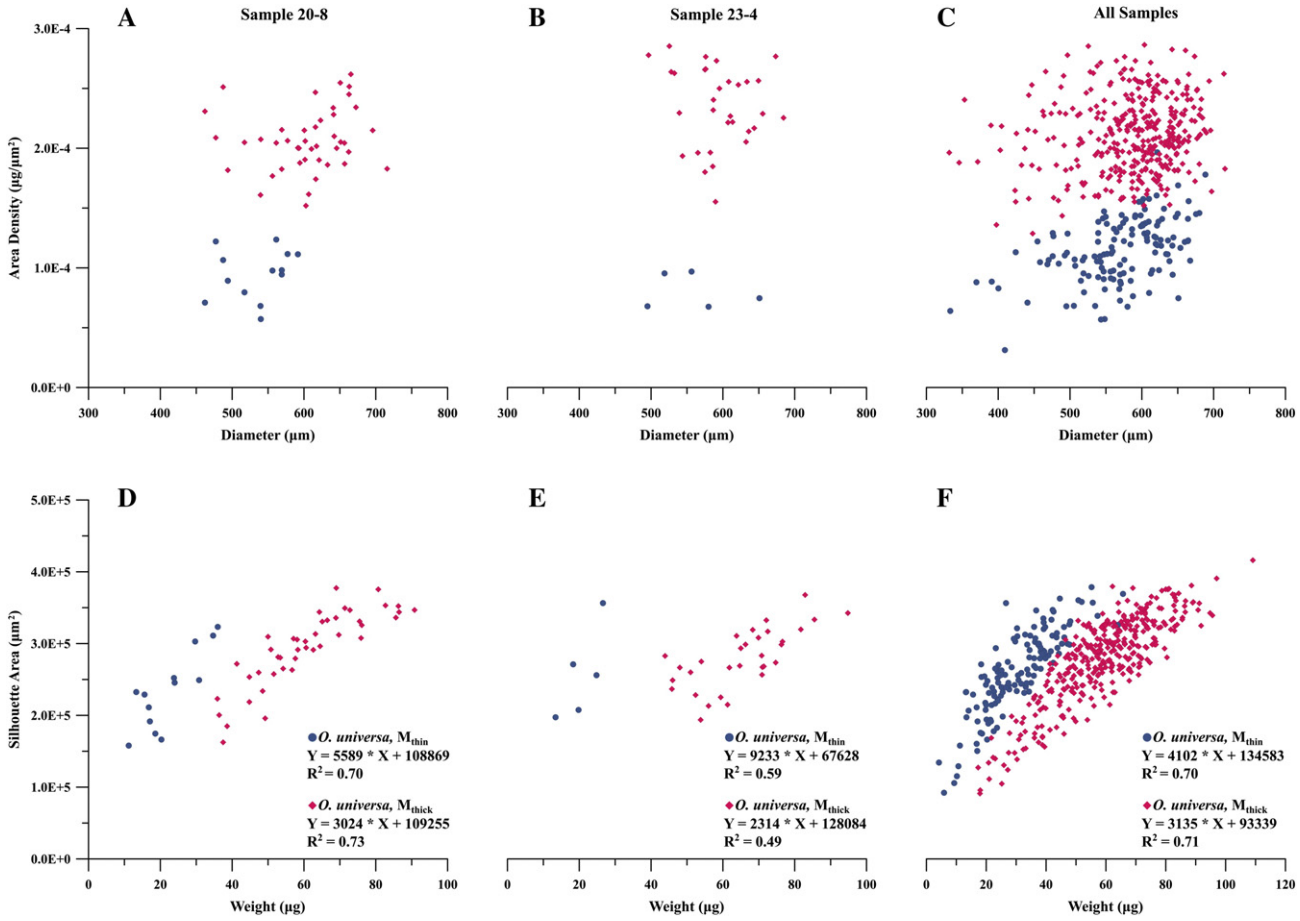

Fig. 3. (A–F). The top plots are *O. universa* M_{thin} (blue circles) and M_{thick} (pink diamonds) area density (ρ_A) and diameter cross plots for sample 20-8 (A), sample 23-4 (B) and all samples (C). The bottom plots are silhouette area and weight cross plots for sample 20-8 (D), sample 23-4 (E) and all samples (F).

2.0 to characterize porosity and thickness variations between the two morphotypes. Porosities were calculated within the maximum region of the inner shell determined to be at a normal angle to the center of the shell. Small and large pores were manually marked and their areas summed. Small, large and total pore areas were divided by the total area of the surveyed region and multiplied by 100 to calculate porosity.

SEM-measured thicknesses were averaged from 5 measurements taken at random along the shell edge. We use the relationships between the area densities and measured thicknesses of samples 20-7 and 22-7 to derive morphotype-specific equations for estimating the thicknesses of M_{thin} and M_{thick} (Tables 2, Fig. 4A and B). These equations were used to calculate thickness for all specimens examined in this study. The porosities and calculated thicknesses were used to characterize the morphotypes and compare them to the previously published porosity and thickness measurements for the three known cryptic species of *O. universa* (Morard et al., 2009). We also used the SEM images to assess whether or not the specimens had undergone gametogenic calcification, defined by the absence of spines (*O. universa* sheds its calcitic spines during gametogenic calcification, leaving only spine bases on the final chamber outer wall; Spero, 1988) and the presence of a thin gametogenic calcite layer on the spine bases (Table 2).

2.5. Estimated calcification depth and temperature

Following the morphometric analyses, groupings of one to eight *O. universa* shells from each morphotype (diameter >500 µm) were analyzed for oxygen and carbon isotopes using a GV IsoPrime stable isotope ratio mass spectrometer (long-term 1σ standard reproducibility is ±0.06‰ for $\delta^{13}C$ and 0.07‰ for $\delta^{18}O$). The isotopic values are reported relative to Vienna Pee Dee Belemnite (V-PDB). Calcification temperatures were estimated from the oxygen isotopic compositions of *O. universa* using the following species-specific equation developed by Bemis et al. (1998):

$$T(^{\circ}C) = 16.5 - 4.80(\delta_c - (\delta_w - 0.27)) \quad (4)$$

where δ_c is the $\delta^{18}O$ of the foraminiferal calcite and δ_w is the $\delta^{18}O$ of the calcifying waters which are scaled from V-SMOW to V-PDB by subtracting 0.27‰. Here, we use the low light (LL) equation because the symbiont P_{max} light levels for *O. universa* (>386 µE m^{-2} s^{-1}; Spero and Parker, 1985) generally occurs in the upper 20 m of the water column in the Cariaco Basin (Lorenzoni et al., 2011), which is shallower than the inferred habitat depth of *O. universa* at this location. δ_w was estimated using the $\delta^{18}O$–salinity relationship for Cariaco Basin (McConnell et al., 2009):

$$\delta_w = 0.34(\pm 0.09) \times (\text{salinity}) - 11.5(\pm 3.4). \quad (5)$$

Calculated calcification temperatures were compared to measured temperatures in order to determine the average calcification depth of the final chamber. Additional measured and calculated hydrographic parameters (e.g., salinity, pH, alkalinity, $[CO_3^{2-}]$, water density, oxygen, nutrient, irradiance and chlorophyll concentrations) at the estimated calcification depth were then used to define the environment of the two *O. universa* morphotypes during the final 2–9 days of calcification. Carbonate ion concentration ($[CO_3^{2-}]$) was calculated using alkalinity,

Table 2
Thickness, porosity, diameter and area density values for samples 20-7 and 22-7.

Sample	Sample #	Morphotype	Gam/pre–gam	Measured thickness (μm)	ρ_A–Calculated Thickness (μm)	Geometric–calculated thickness (μm)	Small porosity (%)	Large Porosity (%)	Total Porosity (%)	Diameter (μm)	ρ_A (1 x 10^4 μg/μm^2)
20_7	1	Thin	P	7.8	11.65	12.32	8.9	0.0	8.9	424.36	1.13
20_7	4	Thin	G	17.1	17.5	17.1	4.0	3.5	7.5	497.16	1.69
20_7	6*	Thin	G	23.0	21.0	20.5	5.8	2.3	8.1	491.83	2.02
20_7	8*	Thin	G	20.0	21.7	21.3	6.2	3.6	9.8	624.49	2.09
20_7	14	Thin	P				7.4	1.4	8.8	575.62	1.07
20_7	23	Thin	P	9.4	14.0	13.9	5.1	3.3	8.5	599.85	1.35
20_7	37	Thin	P	14.2	15.0	14.7	4.9	2.8	7.7	650.02	1.45
20_7	45	Thin	P				7.2	3.3	8.8	577.55	1.41
22_7	15	Thin	G	12.4	11.5	11.4	6.5	3.9	10.1	547.24	1.11
22_7	20	Thin	G	16.8	14.1	14.3				551.22	1.37
22_7	24	Thin	G	16.4	13.3	13.5	3.8	2.6	6.4	539.27	1.29
22_7	25	Thin	G	14.8	12.9	13.1				606.95	1.25
22_7	43	Thin	G	12.2	11.5	11.6	3.0	4.4	7.5	551.69	1.12
20_7	9	Thick	G	36.3	34.7	30.0	6.1	8.4	14.5	629.91	2.57
20_7	10	Thick	G	30.6	33.5	27.0	7.9	7.8	15.7	619.04	2.48
20_7	16	Thick	P	18.2	23.2	19.7	9.5	2.1	11.5	622.77	1.73
20_7	17	Thick	G	26.3	27.4	22.2	6.2	5.3	11.5	636.07	2.04
20_7	18*	Thick	G	16.7	18.2	15.2	11.8	1.9	13.7	573.97	1.38
20_7	20	Thick	P	23.0	26.6	31.6	10.6	3.1	13.7	565.95	1.98
20_7	27	Thick	G	30.6	34.6	26.5	7.2	8.7	15.9	693.76	2.56
20_7	28*	Thick	P	18.6	16.9	14.0	11.1	1.9	13.0	607.98	1.29
20_7	29*	Thick	P	15.6	13.6	11.1	4.8	11.1	15.8	667.32	1.06
20_7	33*	Thick	G	13.6	10.1	8.3	6.2	7.2	13.4	610.12	0.79
22_7	7	Thick	G	24.6	24.6	21.0				629.36	1.84
22_7	9	Thick	G	34.3	26.6	22.2	9.7	5.5	15.3	600.7	1.98
22_7	10	Thick	G	35.6	29.9	24.9	8.1	10.5	18.7	639.62	2.22
22_7	11	Thick	G	25.1	21.8	17.5	8.3	5.1	13.4	697.17	1.64
22_7	13	Thick	G	32.1	29.3	23.7	9.8	10.3	20.0	638.97	2.18
22_7	19	Thick	G	24.7	27.9	23.9	5.2	7.2	12.4	513.88	2.08
22_7	23	Thick	G	32.4	32.8	26.8	7.7	11.3	19.1	597.08	2.43
22_7	26	Thick	G	24.9	24.4	20.5	8.7	6.7	15.4	605.36	1.82
22_7	27*	Thick	P	10.3	13.0	10.4	8.7	2.9	11.6	544.19	1.00
22_7	28	Thick	G	33.1	31.7	28.0				536.81	2.35
22_7	29	Thick	G	17.2	20.2	17.6	6.5	6.7	13.2	603.04	1.52
22_7	30	Thick	G	35.9	31.1	25.3	8.9	10.8	19.6	641.07	2.31
22_7	31*	Thick	G	18.4	18.3	15.3	5.7	7.7	13.4	623.12	1.39
22_7	32	Thick	G	36.1	34.7	28.4	7.8	5.5	13.4	582.5	2.57
22_7	35	Thick	P	19.9	21.2	17.1	12.0	1.8	13.8	588.87	1.59
22_7	36	Thick	G	22.2	21.1	17.2				571.99	1.59
22_7	37*	Thick	P	8.5	9.7	7.5	10.1	2.3	12.5	587.6	0.76
22_7	38	Thick	G	24.5	23.9	20.2	9.8	5.0	14.9	585.4	1.79
22_7	39	Thick	G	22.2	23.6	20.0	10.6	7.1	17.6	623.67	1.76
22_7	41	Thick	G	22.5	22.0	19.7	7.6	5.0	12.6	607.91	2.16
22_7	42	Thick	G	17.4	24.4	12.2	9.0	3.8	12.9	650.22	1.65
Mean M_{thin}				14.9	14.9	14.9	5.7	2.8	8.4	556.7	1.41
1σ M_{thin}				4.4	3.6	3.4	1.8	1.3	1.1	60.7	0.33
Mean M_{thick}				24.2	24.2	20.2	8.4	6.2	14.6	609.5	1.82
1σ M_{thick}				7.9	7.1	6.4	2.0	3.0	2.5	41.0	0.51

[a]Indicates specimens that were misidentified using the morphometric methods presented in this study.

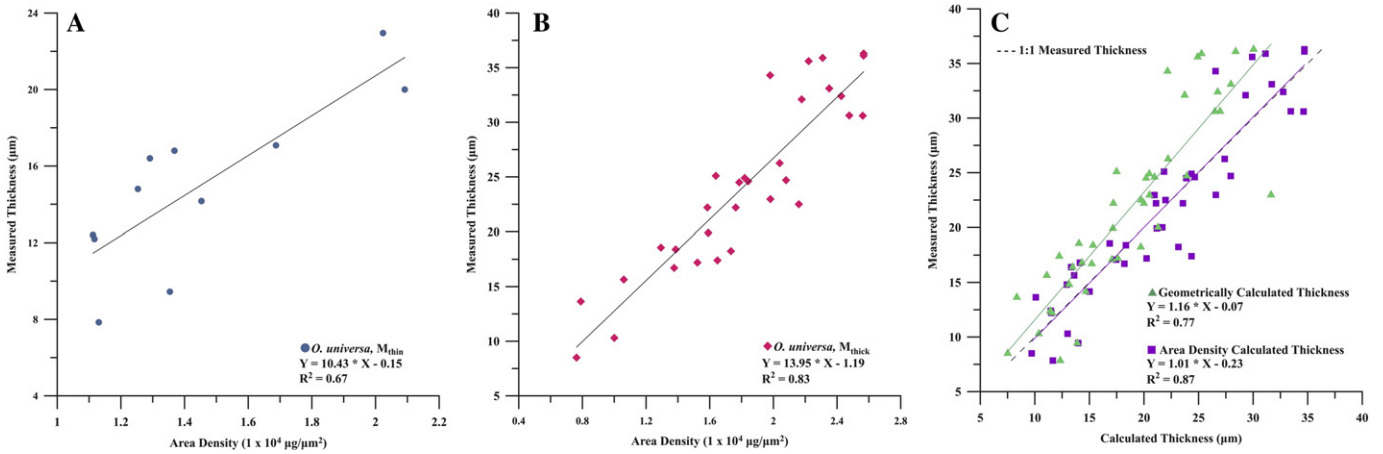

Fig. 4. Area density (ρ_A) and measured thickness relationships for M_{thin} (A; blue circles) and M_{thick} (B; pink diamonds) from samples 20-7 and 22-7. (C) Comparison between geometric (green triangles) and ρ_A (purple squares) thickness calculations.

pH, salinity, temperature and nutrient concentrations and CO2SYS.xls (Pelletier et al., 2007, version 16). In an effort to isolate possible effects of size on $\delta^{18}O$ and $\delta^{13}C$ (Bouvier-Soumagnac and Duplessy, 1985; Elderfield et al., 2002; and Friedrich et al., 2012), the isotopic measurements were restricted to shells with diameters between 540 and 665 µm.

3. Results

3.1. Biometric characteristics

We find two biometrically distinct *O. universa* morphotypes in the CARIACO sediment trap samples, which are easily differentiated by thin (M_{thin}) and thick (M_{thick}) shell walls. All morphometric data is summarized in Table 3. The mean silhouette areas of the M_{thin} and M_{thick} are 2.64 (±0.54) and 2.75 (±0.63) × 10^5 µm², respectively, and are not significantly different (paired comparison T-test; $p = 0.330$, $t = -1.01$). Measured diameters were also similar for the two morphotypes, ranging between 330 and 688 µm for M_{thin} (mean = 570 µm) and 330 and 715 µm for M_{thick} (mean = 585 µm; $p = 0.284$, $t = -1.12$). In contrast, the mean weights for the two morphotypes are significantly different from one another, with a mean weight of 32 (±10; range = 4–66) µg for M_{thin} and 59 (±13, range = 17–110) µg for M_{thick} ($p = 0.000$, $t = -8.94$). Because the two morphotypes exhibit similar mean diameters, the weight differences must be a result of a difference in shell thickness. Indeed, significant differences in the mean area densities (ρ_A; M_{thin} = 1.16 (±0.22) × 10^4 µg/µm², M_{thick} = 2.13 (±0.28) × 10^4 µg/µm²) and calculated thicknesses (M_{thin} = 13 (±2; range = 6–22) µm, M_{thick} = 28 (±4; range = 19–41) µm) of the two morphotypes indicate that M_{thick} is characterized by a thicker shell wall ($p = 0.000$, $t = -13.16$ for ρ_A; $p = 0.000$, $t = -17.56$ for thickness).

The SEM-measured shell thickness and porosity values for sediment trap samples 20-7 and 22-7 can be found in Table 2. Sample images of both morphotypes, including those of the pores and shell edges, are presented in Fig. 5. Examination of shell wall images revealed that pre-gametogenic individuals are present in both morphotype groups, being more abundant for M_{thin} than M_{thick} (38% vs. 23%, respectively; Table 2).

The SEM measured and calculated thicknesses agree on average within 0.1 µm (Table 2, n = 40), indicating that the ρ_A–thickness equations for the two morphotypes are effective at estimating *O. universa* shell thickness (Table 2). The imaged M_{thin} specimens have an average porosity of 8% (±1; range = 6–10%, n = 11), while M_{thick} specimens have an average porosity of 15% (±2.5; range = 11–20%, n = 28) and differ significantly from one another ($p = 0.000$, $t = -8.750$). Relative to M_{thin}, M_{thick} is characterized by higher average small (8.4% vs. 5.7%) and large porosities (14.6% vs. 8.4%; Fig. 6). The two morphotypes exhibit a similar range in small porosities (M_{thin} = 3.0–8.9%; M_{thick} = 4.8–12.0%), thus, the majority of the porosity differences between the two morphotypes can be attributed to differences in the area of large pores (M_{thin} = 0.0–4.4%; M_{thick} = 1.8–11.3%; Fig. 6).

3.2. Accuracy of morphometric method

Unlike thickness, which increases continually for *O. universa* after the final spherical chamber has been secreted (Spero et al., 2015), pore distribution remains constant once the final chamber has been fully formed (Spero, 1998). Though the apparent porosity would be greater on the outer surface of thicker shells as pore walls angle outwards toward the surface of the shell (Spero et al., 1998), porosity measurements on the inner shell wall are representative of the pore distribution at the time of initial chamber calcification. If we assume that inner shell porosity is the most defining and constant characteristic for distinguishing between morphotypes/genotypes in a given region (Morard et al., 2009), we can use the porosity measurements for samples 20-7 and 22-7 to determine the accuracy of the ρ_A method for identifying M_{thick} as M_{thin}. Morard et al. (2009) report porosities ranging from 12–30% and 6–10% for the Caribbean and Mediterranean cryptic species collected from the C-MarZ sites, respectively. If we divide the porosity measurements for samples 20-7 and 22-7 (Table 2) into comparable ranges, we find that approximately 85% of M_{thin} have porosities that fall within the lower porosity range (6–10%) and 77% of M_{thick} have porosities that fall within the higher porosity range (11–20%). Thus, the morphometric method presented in this study correctly identifies the *O. universa* morphotypes 77–85% of the time. We suspect that the main cause for the misidentification of *O. universa* M_{thick} as M_{thin} is the absence of gametogenic calcite in M_{thick}, which would affect both the area density and weight–area relationships of a specimen. Indeed, we find that more than 50% of the misidentified M_{thick} specimens had not undergone gametogenic calcification based on the SEM images of the shell wall (Table 2). The two M_{thin} specimens misidentified as M_{thick} have anomalously thick shell walls as compared with those observed from the other M_{thin} specimens. In summary, using porosity as a separate, and likely more constant biometric attribute than thickness, the ρ_A method identified the correct morphotype for ~80% of the *O. universa* specimens, with the majority of misidentifications attributed to the absence of gametogenic calcite in the M_{thick} group.

Compared to earlier geometric methods for calculating shell thickness in *O. universa* (see Billups and Spero, 1995 for method description), we find that the ρ_A method presented in this study is more effective at

Table 3
Morphometrics for *O. universa* morphotypes.

Area

Sample ID	Trap date	All morphotypes area (1×10^{-5} μm^2)	1σ	M_{thin} area (1×10^{-5} μm^2)	1σ	M_{thick} area (1×10^{-5} μm^2)	1σ
19_5	7/13/2005	2.61	5.60	2.99	4.08	2.46	5.52
19_8	8/24/2005	2.39	6.70	2.62	5.14	2.34	6.96
19_11	10/5/2005	2.50	5.13	2.79	4.76	2.33	4.90
20_7	2/7/2006	2.87	5.42	2.71	5.09	2.92	5.49
20_8	2/21/2006	2.82	5.79	2.34	5.45	2.94	5.19
21_3	6/14/2006	2.81	6.78	0.00	0.00	2.81	6.78
21_8	8/23/2006	2.70	5.77	2.57	6.23	2.82	4.89
21_13	11/1/2006	2.49	5.80	2.04	6.86	2.66	4.52
22_1	11/8/2006	2.76	4.03	2.79	4.35	2.66	3.24
22_7	1/31/2007	2.70	6.16	2.42	6.73	2.84	24.22
22_9	2/28/2007	2.53	6.53	2.31	6.82	2.64	6.21
23_1	5/16/2007	3.29	3.72	3.31	6.15	3.29	3.48
23_4	6/27/2007	2.77	4.46	2.58	6.34	2.80	4.14
23_11	10/3/2007	2.63	4.62	2.71	4.55	2.56	4.69
24_4	1/8/2008	2.99	4.17	2.81	3.65	3.12	4.18
Mean		2.72	5.38	2.46	5.08	2.75	6.29

Diameter

Sample ID	Trap date	All morphotypes diameter (μm)	1σ	M_{thin} diameter (μm)	1σ	M_{thick} diameter (μm)	1σ
19_5	7/13/2005	565.00	64.35	608.39	38.27	548.75	65.64
19_8	8/24/2005	584.20	83.19	571.84	50.19	531.66	87.88
19_11	10/5/2005	577.06	60.76	585.74	52.40	533.20	59.93
20_7	2/7/2006	597.52	58.94	581.47	62.54	602.59	57.69
20_8	2/21/2006	608.16	64.70	543.76	64.38	605.07	58.34
21_3	6/14/2006	615.57	77.69			615.57	77.69
21_8	8/23/2006	599.82	64.93	564.51	72.47	593.68	53.99
21_13	11/1/2006	576.91	67.38	505.41	88.95	580.14	45.98
22_1	11/8/2006	581.78	43.29	564.17	31.51	587.07	46.30
22_7	1/31/2007	576.78	73.70	546.38	78.55	592.63	70.36
22_9	2/28/2007	588.15	79.05	528.28	90.06	571.96	70.127
23_1	5/16/2007	637.90	38.35	641.68	70.06	637.45	34.65
23_4	6/27/2007	594.99	47.90	560.21	60.44	594.19	44.99
23_11	10/3/2007	583.97	49.92	583.73	46.64	564.85	52.24
24_4	1/8/2008	616.48	39.83	600.90	40.13	618.26	35.83
Mean		594	61	570	60	585	57

Weight

Sample ID	Trap date	All morphotypes weight (μg)	1σ	M_{thin} weight (μg)	1σ	M_{thick} weight (μg)	1σ
19_5	7/13/2005	54.07	14.93	50.14	11.28	55.58	16.27
19_8	8/24/2005	44.07	16.38	32.33	11.72	44.07	16.38
19_11	10/5/2005	45.37	14.19	33.81	8.85	51.49	12.67
20_7	2/7/2006	57.01	20.47	32.46	20.47	64.76	16.35
20_8	2/21/2006	54.39	21.19	24.18	8.15	61.59	14.69
21_3	6/14/2006	62.57	19.28			62.57	19.28
21_8	8/23/2006	48.65	18.25	32.05	11.16	58.13	11.57
21_13	11/1/2006	45.43	19.54	19.88	11.50	55.25	10.97
22_1	11/8/2006	37.30	17.25	29.21	8.72	64.27	4.97
22_7	1/31/2007	45.78	19.77	26.98	11.57	57.34	12.26
22_9	2/28/2007	42.64	18.28	27.19	13.89	49.73	15.61
23_1	5/16/2007	68.75	14.87	49.60	17.28	71.00	13.09
23_4	6/27/2007	59.32	19.69	20.58	5.28	65.57	12.58
23_11	10/3/2007	42.71	12.37	33.82	7.22	50.71	10.45
24_4	1/8/2008	52.96	20.56	32.38	6.36	67.93	12.14
Mean		50.73	17.80	31.76	10.96	58.66	13.28

Area density

Sample ID	Trap date	All morphotypes ρ_A (1×10^4 μg/μm^2)	1σ	M_{thin} ρ_A (1×10^4 μg/μm^2)	1σ	M_{thick} ρ_A (1×10^4 μg/μm^2)	1σ
19_5	7/13/2005	2.07	3.98	1.66	1.87	2.22	3.43
19_8	8/24/2005	1.84	4.06	1.21	2.55	1.99	2.72
19_11	10/5/2005	1.85	5.34	1.20	1.39	2.19	2.64
20_7	2/7/2006	1.96	5.39	1.19	2.59	2.19	3.38
20_8	2/21/2006	1.81	5.38	0.95	2.09	2.07	2.60
21_3	6/14/2006	2.21	3.23	0.00	0.00	2.21	3.23
21_8	8/23/2006	1.76	5.14	1.23	1.72	2.07	2.60
21_13	11/1/2006	1.76	5.58	0.95	2.82	2.07	1.78
22_1	11/8/2006	1.35	6.33	1.03	1.56	2.43	1.93
22_7	1/31/2007	1.66	5.45	1.05	3.03	1.98	3.14
22_9	2/28/2007	1.62	4.56	1.13	3.25	1.88	2.62
23_1	5/16/2007	2.07	3.26	1.46	3.03	2.13	2.45
23_4	6/27/2007	2.14	6.26	0.80	1.46	2.35	3.34
23_11	10/3/2007	1.65	4.79	1.25	1.50	2.00	3.74

(continued on next page)

Table 3 *(continued)*

Area density							
Sample ID	Trap date	All morphotypes ρ_A (1×10^4 μg/μm^2)	1σ	M_{thin} ρ_A (1×10^4 μg/μm^2)	1σ	M_{thick} ρ_A (1×10^4 μg/μm^2)	1σ
24_4	1/8/2008	1.75	5.59	1.15	1.69	2.18	2.29
Mean		1.83	4.96	1.08	2.04	2.13	2.79
Calculated thickness							
Sample ID	Trap date	All morphotypes thickness (μm)	1σ	M_{thin} thickness (μm)	1σ	M_{thick} thickness (μm)	1σ
19_5	7/13/2005	26.32	7.19	17.25	2.05	30.86	3.26
19_8	8/24/2005	24.08	6.33	13.26	2.51	26.55	3.79
19_11	10/5/2005	24.14	8.36	13.06	1.34	29.35	3.68
20_7	2/7/2006	25.29	8.17	16.65	4.74	27.41	6.33
20_8	2/21/2006	23.73	7.96	10.69	2.06	27.67	3.63
21_3	6/14/2006	29.63	4.51			29.63	4.51
21_8	8/23/2006	23.42	7.27	13.48	1.70	27.64	3.63
21_13	11/1/2006	23.01	8.24	10.69	2.78	27.75	2.48
22_1	11/8/2006	16.40	9.44	11.51	1.54	32.68	2.69
22_7	1/31/2007	21.72	8.40	9.96	1.63	24.93	6.03
22_9	2/28/2007	20.75	6.94	12.54	3.21	25.04	3.65
23_1	5/16/2007	27.39	5.24	15.77	2.99	28.56	3.42
23_4	6/27/2007	28.51	8.95	9.29	1.44	31.61	4.67
23_11	10/3/2007	20.76	7.69	13.68	1.52	26.78	5.22
24_4	1/8/2008	22.28	8.77	12.72	1.81	29.24	3.20
Mean		23.83	7.56	12.90	1.67	28.38	4.01

accurately estimating shell thickness, particularly for thicker shells (Fig. 4C). This may be due to the necessity of applying a porosity correction to geometrically calculated thickness, which is a morphometric trait that varies among the morphotypes and cryptic species of *O. universa* (Morard et al., 2009; this study). Though we applied porosity corrections using the average porosities for each morphotype (M_{thin} = 8%, M_{thick} = 15%), we found that the geometrically determined thicknesses progressively underestimated measured thicknesses as shell thickness increased.

3.3. Seasonal changes in morphotype abundances

The abundances and fluxes of M_{thin} and M_{thick} are listed in Table 1. M_{thick} is the more abundant of the two morphotypes, comprising on average 75% of the total *O. universa* specimens in the sediment trap samples. When comparing the fluxes of M_{thin} and M_{thick} to the time-equivalent monthly averaged upwelling index (Astor et al., 2013), we find that the fluxes of M_{thick} are higher during upwelling periods, with mean upwelling fluxes of 17 shells/m/day and mean non-upwelling fluxes of 9 shells/m/day (Fig. 7). In contrast, there is no difference in flux for M_{thin} between upwelling and non-upwelling periods (mean flux upwelling = 5 shells/m/day, mean flux non-upwelling = 5 shells/m/day). However, we observe the lowest fluxes in M_{thin} during peak upwelling periods (samples 21-3 (0 shells/m/day) and 23-1 (2 shells/m/day)).

3.4. Oxygen and carbon isotopes

The bulk (average of both morphotypes) and morphotype-specific oxygen and carbon isotopic data for *O. universa* are listed in Table 4. The sample means presented in Table 4 are weighted based on the number of individuals per sample analysis in order to give more weight to those samples containing more *O. universa* individuals. A paired comparison T-test revealed that for both carbon and oxygen isotopes, the differences between M_{thin} and M_{thick} are highly significant ($t = 4.390$, $p = 0.001$ and $t = -5.294$, $p = 0.000$ for $\delta^{13}C$ and $\delta^{18}O$, respectively). The $\delta^{18}O$ and $\delta^{13}C$ of M_{thick} are on average 0.34‰ higher and 0.38‰ lower, respectively, than those of M_{thin} (Figs. 8 and 9). The offset in $\delta^{18}O$ and $\delta^{13}C$ values of M_{thin} and M_{thick} is higher during non-upwelling periods ($\delta^{18}O$ offset = −0.54‰; $\delta^{13}C$ offset = 0.41‰) relative to upwelling periods ($\delta^{18}O$ offset = −0.15‰; $\delta^{13}C$ offset = 0.25‰; Fig. 10, see discussion Section 4.2 for further explanation).

3.5. Final chamber calcification depths and hydrographic parameters

The mean $\delta^{18}O$ values from each sample were used to calculate calcification temperatures for the individual morphotypes using Eqs. 4 and 5 (Table 5). M_{thin} and M_{thick} had average calcification temperatures for the final *O. universa* chamber of 23.3 and 21.6 °C, respectively, which are within the optimal temperature range proposed for *O. universa* (22–28 °C; Caron et al., 1987; Lombard et al., 2009). However, the two morphotypes have distinctly different average depths at which the final spherical chamber calcifies, with M_{thick} calcifying at deeper depths (25–130 m) than M_{thin} (7–100 m; Fig. 2). Specifically, M_{thick} is adding its final chamber in waters characterized by lower temperatures (21–23 °C), pH (7.85–8.01), [O_2] (100–175 μmol/kg) and chlorophyll concentrations (0–750 ng/L). Final chamber calcification for M_{thin} occurs at higher temperatures (mean = 22–24 °C), pH (mean = 7.93–8.04), [O_2] (100–200 μmol/kg), and chlorophyll concentrations (60–830 ng/L) (Table 5). Salinities at the estimated calcification depths for both morphotypes are very similar and closely correspond with the salinity maximum in the basin (36.8).

The calcification depths for both morphotypes varied throughout the 3-year study period, with both calcifying at shallower depths during upwelling periods (Fig. 2). Differences in the depths of calcification for the two morphotypes tend to be small during periods of upwelling, and increase during periods of non-upwelling and enhanced stratification. Temperature, salinity and density (σ_T) were relatively constant at the depth of calcification for each species over the study period (Table 5; Fig. 2). In contrast, chlorophyll concentrations were more variable at the estimated depths of calcification for both morphotypes, but consistently higher for M_{thin} (mean Chl = 400 vs. 300 ng/L for M_{thick}).

4. Discussion

4.1. Morphotype identification

The morphometric methods presented here are effective at differentiating between *O. universa* morphotypes, which are not readily distinguishable under a simple stereo binocular microscope. SEM imaging, while an effective way of distinguishing *O. universa* genotypes (Morard et al., 2009), is destructive to the shell and does not allow for subsequent geochemical analysis. The ρ_A methods provides a non-destructive means by which *O. universa* genotypes can be distinguished

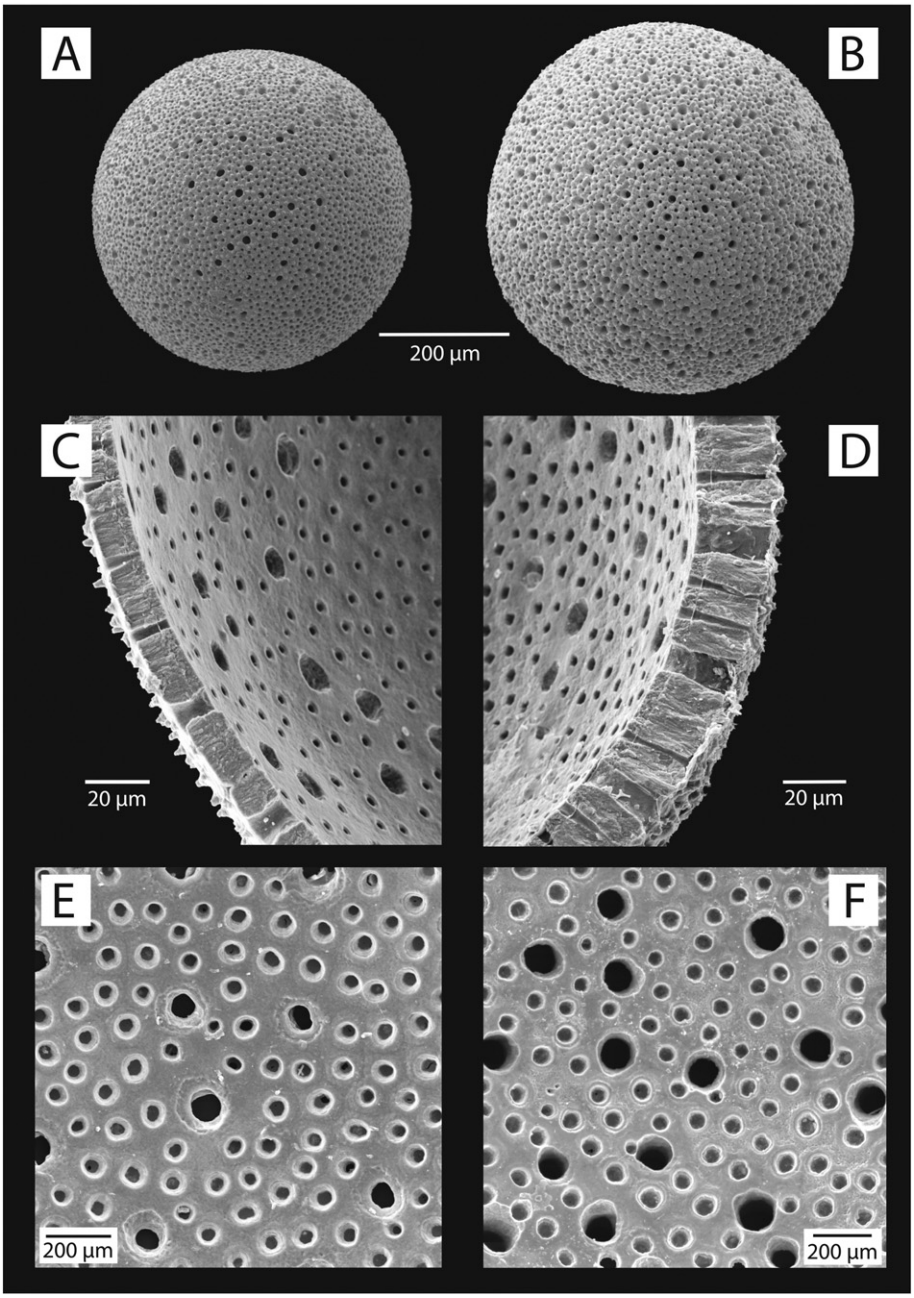

Fig. 5. SEM images of M_{thin} (A) and M_{thick} (B) whole specimen. M_{thin} (C) and M_{thick} (D) shell edge. M_{thin} (E) and M_{thick} (F) inner surface.

from one another, allowing for subsequent geochemical analysis. Though we acknowledge that changes in temperature, food availability, light intensity and carbonate ion concentration ($[CO_3^{2-}]$) likely influence the morphometrics of the *O. universa* final chamber (Bé et al., 1973; Lea et al., 1995; Barker and Elderfield, 2002; Schmidt et al., 2004; Lombard et al., 2009, 2010; Marshall et al., 2013), these factors do not appear to inhibit the identification of thin and thick *O. universa* morphotypes using the methods presented in this study. If only a single morphotype exists in a given sample, it is possible to assign an *O. universa* specimen to a morphotype by comparing its mean weight, area and ρ_A to the ranges exhibited by thick and thin morphotypes in a given study area (Fig. 3C and F). This method was particularly useful for the single morphotype specimens from sample 21-3, which were determined to be M_{thick} based on their morphometric characteristics. The final chamber characteristics of *O. universa* morphotypes likely vary regionally due to differences in the above-mentioned environmental factors known to influence final chamber morphometrics. Thus, researchers should use caution when comparing the biometric characteristics of *O. universa* morphotypes from different study areas.

The porosity differences exhibited by the thin and thick morphotypes may be a result of ecophenotypic and/or genetic controls (Fig. 6). In foraminifera, small pores are used for gas transport, while large pores are used for food/digestion byproducts and symbiont movement into and out of the organism (Bé et al., 1980; Spero, 1987, 1988). Small and large pore distribution is set at the time of initial sphere calcification (Table 2; Spero, 1988). Differences in large porosities between the two morphotypes may be attributed to differences in food supply, prey size and/or symbiont density during the juvenile, trochospiral shell phase of the organism, while differences in smaller porosity may be attributed to changes in gas concentrations (e.g., oxygen) in their respective final chamber calcification environments. However, higher large and small porosities in M_{thick} relative to M_{thin} are inconsistent

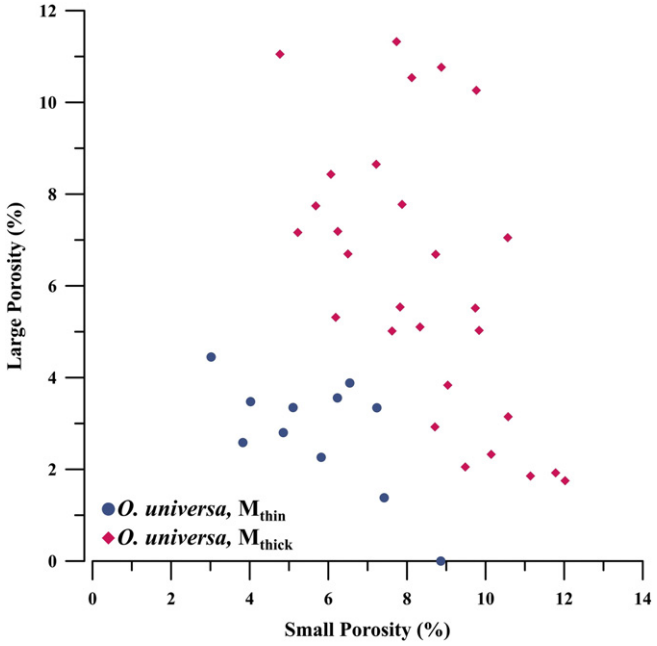

Fig. 6. Small and large porosity distributions for M_{thin} (blue circles) and M_{thick} (pink diamonds).

with some of these ecophenotypic concepts. For example, oxygen concentrations are supersaturated and are on average within 23 μmol/kg at the calcification depths of the two morphotypes, suggesting that small porosities should be comparable between the two morphotypes (Table 5).

Porosity differences could also be attributed to genetic differences between the two morphotypes (Morard et al., 2009). Although genetic testing could not be performed on the *O. universa* morphotypes in this study due to the preservation of sediment trap samples in formalin, we use the phenotypic characteristics of the three identified cryptic species of *O. universa* (de Vargas et al., 1999; Morard et al., 2009, 2013) to infer the genetic variety of the two morphotypes recognized in our study. Morard et al. (2009) report the presence of all three cryptic species of *O. universa* at the C-MarZ sampling sites in the Caribbean Sea, although only two Sargasso specimens were reported for these locations. Due to the high productivity in the Cariaco Basin (Muller-Karger et al., 2001) and the fact that the Sargasso cryptic species is only found in great abundances in the oligotrophic regions of the world's oceans (de Vargas et al., 1999), we think it is highly unlikely that this cryptic species is present in the Cariaco Basin. The biometrics of M_{thin} are characteristic of the Mediterranean cryptic species described at the nearby C-MarZ sampling site (mean thickness = 6 (±2.5) μm, range = 2–10 μm; mean porosity = 8 (±0.01) %, range = 6–10%), while M_{thick} is defined by biometrics comparable to those of the Caribbean cryptic species (mean thickness = 21 (±6.8) μm, range = 5–27 μm; mean porosity = 19 (±4) %; range = 12–25%). Additionally, the temperature (21–27 °C; Fig. 2) and chlorophyll concentrations (350 vs. 250 ng/L) in the Cariaco Basin surface waters over the study period are optimal for the presence of both species (de Vargas et al., 1999; Morard et al., 2009, 2013). Based on morphometrics and the hydrographic conditions of the Cariaco surface waters, we conclude that M_{thin} and M_{thick} are the Mediterranean and Caribbean cryptic species, respectively.

4.2. Oxygen and carbon isotopic variability

We find that a relationship exists between the offset in $\delta^{18}O$ and $\delta^{13}C$ values of M_{thin} and M_{thick} and the relative stratification of the upper water column, inferred from the monthly upwelling index anomaly (Fig. 10; Astor et al., 2013). The offset between the $\delta^{18}O$ and $\delta^{13}C$ of M_{thin} and M_{thick} covaries well with the monthly upwelling index anomaly, with the offset in $\delta^{18}O$ and $\delta^{13}C$ between M_{thin} and M_{thick} increasing during periods of non-upwelling. The exception is with sample 23-1 ($\delta^{13}C$ only), which was one of three samples that only contained enough M_{thin} individuals for a single sample analysis. Additionally, scatter (1σ) of the *O. universa* $\delta^{18}O$ and $\delta^{13}C$ (Table 4; Fig. 8) increases slightly during non-upwelling periods (1σ = 0.38 and 0.33‰ for $\delta^{13}C$ and $\delta^{18}O$, respectively) relative to upwelling periods (1σ = 0.31 and 0.27‰ for $\delta^{13}C$ and

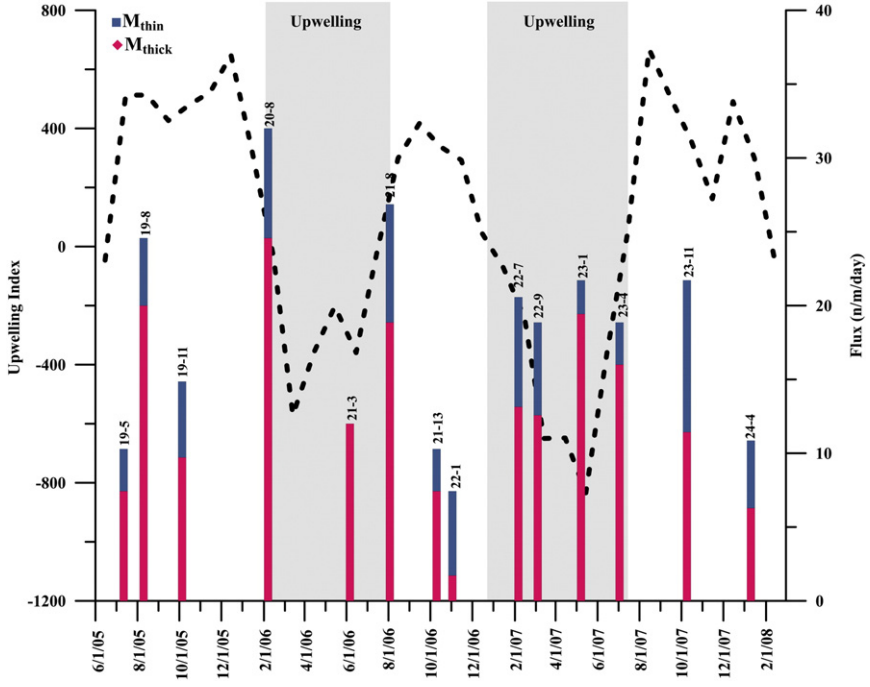

Fig. 7. M_{thin} (blue) and M_{thick} (pink) fluxes and monthly averaged upwelling index record spanning the sample collection period with associated sample IDs.

Table 4
Oxygen and carbon isotopic compositions for M_{thin} and M_{thick}. All means are weighted to the number of individuals per sample analysis (n).

Sample Name	Both morphotypes $\delta^{13}C$ (‰)	Both morphotypes $\delta^{18}O$ (‰)	n[b]	M_{thin}	$\delta^{13}C$ (‰)	$\delta^{18}O$ (‰)	n	Mean Thickness (μm)	Mean Diameter (μm)	M_{thick}	$\delta^{13}C$ (‰)	$\delta^{18}O$ (‰)	n	Mean Thickness (μm)	Mean Diameter (μm)
CAR 19-5					1.79	-0.73	4	17.7	578		1.45	-0.36	3	32.8	570
											1.41	-0.71	4	31.5	578
MEAN[a]	1.56	-0.62	11		1.79	-0.73		18	578		1.43	-0.56		32	575
1σ	0.21	0.21									0.03	0.24		1	6
CAR 19-8					1.35	-0.51	3	14.0	592		0.65	-0.11	1	25.1	608
					1.51	-0.96	5	12.5	554		0.47	-0.12	1	27.8	616
											0.88	-0.02	3	33.3	601
											0.87	-0.37	7	23.7	576
MEAN	1.08	-0.46	20		1.45	-0.79		13	568		0.82	-0.24		27	588
1σ	0.40	0.35			0.12	0.32		1	27		0.20	0.15		4	17
CAR 19-11					1.90	-1.37	1	14.4	586		0.39	0.00	1	28.7	580
					1.60	-0.67	7	13.3	585		1.17	-0.8	4	34.6	542
											0.92	-0.21	5	28.7	544
MEAN	1.27	-0.44	18		1.64	-0.76		13	585		0.97	-0.18		31	547
1σ	0.59	0.55			0.21	0.49		1	1		0.39	0.11		3	21
CAR 20-8					0.91	-0.40	1	12.3	636		0.97	-0.48	1	28.1	642
					1.17	-0.36	8	10.2	554		1.07	-0.03	1	31.4	641
											1.23	-0.33	3	32.9	576
											1.27	-0.73	4	33.4	666
											0.97	-0.19	5	26.7	593
MEAN	1.13	-0.38	23		1.14	-0.37		10	563		1.12	-0.38		30	617
1σ	0.14	0.22			0.18	0.03		1	58		0.14	0.27		3	38
CAR 21-3											1.35	-0.85	1	27.6	644
											0.67	-0.19	1	28.8	556
											1.17	-0.42	1	34.1	556
											1.79	-0.49	3	28.5	583
											1.06	-0.11	3	33.3	591
											1.06	-0.58	5	26.9	636
											1.22	-0.75	6	26.5	606
MEAN	1.22	-0.53	20								1.22	-0.53		28	605
1σ	0.34	0.27									0.34	0.27		3	35
CAR 21-8					1.64	-0.93	4	14.7	648		0.97	-0.36	1	32.6	635
					1.33	-0.41	5	13.1	594		1.62	-0.59	3	31.1	582
											0.78	-0.47	6	26.5	643
MEAN	1.25	-0.56	19		1.47	-0.64		14	618		1.05	-0.49		29	624
1σ	0.38	0.23			0.22	0.37		1	38		0.44	0.11		3	33
CAR 21-13					2.07	-0.61	1	14.7	599		1.45	-0.32	4	26.6	569
					1.29	-0.98	1	10.3	546		0.79	-0.32	5	28.8	609
MEAN	1.19	-0.41	11		1.68	-0.80		12	573		1.08	-0.32		28	591
1σ	0.53	0.31			0.55	0.26		3	37		0.47	0.00		2	28
CAR 22-1					1.67	-1.03	7	11.0	575		1.16	-0.41	3	32.7	564
MEAN	1.51	-0.84	10		1.67	-1.03		11	575		1.16	-0.41		33	564
1σ	0.36	0.44													

(continued on next page)

Table 4 *(continued)*

Sample Name	Both morphotypes $\delta^{13}C$ (‰)	Both morphotypes $\delta^{18}O$ (‰)	n	M_{thin}	$\delta^{13}C$ (‰)	$\delta^{18}O$ (‰)	n	Mean Thickness (μm)	Mean Diameter (μm)	M_{thick}	$\delta^{13}C$ (‰)	$\delta^{18}O$ (‰)	n	Mean Thickness (μm)	Mean Diameter (μm)
CAR 22-9					0.69	-1.23	1	9.5	569		0.86	0.07	1	24.0	571
					1.93	-0.70	1	13.5	636		1.05	-0.46	1	29.8	570
					1.52	-0.44	5	15.6	583		1.71	-0.33	1	27.1	638
											1.25	0.09	4	24.7	578
											1.14	-0.32	5	26.0	625
MEAN	1.29	-0.32	19		1.46	-0.59		14	589		1.19	-0.16		26	601
1σ	0.42	0.42			0.63	0.41		3	35		0.32	0.25		2	33
CAR 23-1					1.95	-0.68	4	15.8	642		1.23	-0.36	3	31.9	604
											1.34	-0.68	4	31.1	600
											1.06	-0.58	5	27.3	636
MEAN	1.38	-0.59	16		1.95	-0.68		16	642		1.20	-0.56		30	616
1σ	0.39	0.15									0.14	0.16		2	20
CAR 23-4					0.80	-0.46	1	10.9	556		1.13	-0.77	1	26.2	565
											0.23	-0.16	1	25.8	644
											0.87	-0.33	1	35.9	575
											0.44	-0.51	1	34.6	650
											0.89	-0.18	3	37.6	564
											1.07	-0.20	3	27.0	590
											0.77	-0.91	3	29.3	632
											0.82	-0.39	5	34.1	587
MEAN	0.83	-0.42	19		0.80	-0.46		11	556		0.83	-0.42		32	596
1σ	0.29	0.26									0.30	0.28		5	36
CAR 23-11					0.79	-1.13	1	14.0	586		0.97	-0.71	1	26.4	573
					0.70	-1.01	1	14.2	565		1.04	-0.73	1	36.9	565
					1.92	-1.61	1	15.4	591		1.34	-0.60	1	29.6	585
					1.19	-1.05	7	13.8	555		1.40	-0.32	3	31.3	578
					1.45	-0.94	6	12.8	598		1.20	-0.43	4	21.5	564
											0.80	-0.45	6	24.0	605
MEAN	1.17	-0.76	32		1.28	-1.05		14	576		1.07	-0.46		26	584
1σ	0.36	0.38			0.50	0.27		1	18		0.23	0.16		6	15
CAR 24-4					1.62	-1.18	1	11.8	639		0.80	-0.49	1	28.2	639
					1.49	-0.82	6	13.2	588		1.07	-0.36	3	30.7	579
MEAN	1.32	-0.70	11		1.50	-0.87		13	595		1.00	-0.39		30	594
1σ	0.19	0.18			0.07	0.18		1	36		0.13	0.07		2	42
MEAN (All Samples)	1.25	-0.54	18		1.49	-0.73		13	585		1.09	-0.39		29	597
1σ (All Samples)	0.35	0.31			0.31	0.29		2	31		0.26	0.17		3	27

[a] All means are weighted to the number of individuals per sample analysis.
[b] Number of individuals per sample analysis.

$\delta^{18}O$, respectively). Increased scatter in the stable isotopic values of the *O. universa* morphotypes during non-upwelling periods could be attributed to the occurrence of individuals at different depths due to enhanced stratification. This could explain the slight isotopic differences (<0.2‰) exhibited between the non-upwelling sample populations of 21-13 and 22-1, which were collected only 1–3 weeks apart. Interestingly, Deuser (1987) reports similar findings stating that the differences between the $\delta^{18}O$ of the thin and thick morphotypes of *O. universa* from the Sargasso Sea decreased when the surface mixed layer reached depths of 75–100 m.

The cause for the isotopic differences exhibited between M_{thin} and M_{thick}, as well as the relationship between the isotopic differences and surface ocean stratification, can be best explained by a difference in the average final chamber calcification depth of the *O. universa* morphotypes. As previously reported in Billups and Spero (1995), we find no significant relationship between the stable isotopic compositions and *O. universa* shell diameter (Fig. S1) and thickness (Fig. S2) for thin and thick morphotype groups when considered separately, implying that there is no size or diameter influence on stable isotopic compositions of individual morphotypes. Additionally, the differences in the

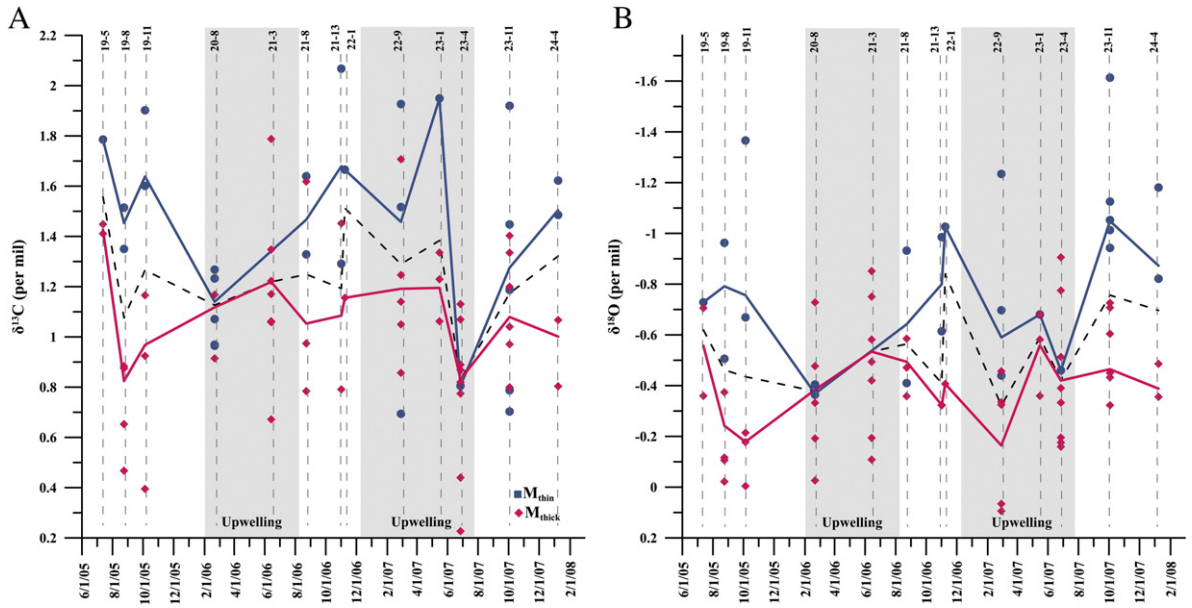

Fig. 8. (A–B). Carbon (A) and oxygen (B) isotopic compositions for *O. universa* M_{thin} (blue circles) and M_{thick} (pink diamonds) throughout the study period (n = 13). The solid blue and pink lines represent the weighted means of M_{thin} and M_{thick}, respectively, based on the number of individuals used per sample analysis (Table 4). The dashed black line represents the weighted mean of all measured specimens and best represent the values that would be generated when lumping the two morphotypes during stable isotopic analysis.

isotopic compositions of the two morphotypes cannot be explained by seasonal differences in occurrence, as both forms are present throughout the year. The $\delta^{18}O$ composition of *O. universa* is primarily a function of temperature in the Cariaco Basin as salinity, and thus $\delta^{18}O_w$, is relatively constant (Table 5). Changes in irradiance (Spero, 1992) and pH/$[CO_3^{2-}]$ (Spero et al., 1997; Bemis et al., 1998; Wolf-Gladrow et al., 1999) may also influence the $\delta^{18}O$ compositions of the two morphotypes. However, the combined effects of $[CO_3^{2-}]$ and irradiance are minimal on the $\delta^{18}O$ of *O. universa*, with a maximum decrease in $\delta^{18}O$ of 0.30 to 0.33‰ under high light (386 μEinst m^{-2} s^{-1}) relative to low light scenarios and a decrease in $\delta^{18}O$ of 0.14‰ for a $[CO_3^{2-}]$ increase of 60 μmol/kg (maximum offset for the two morphotypes, Table 5).

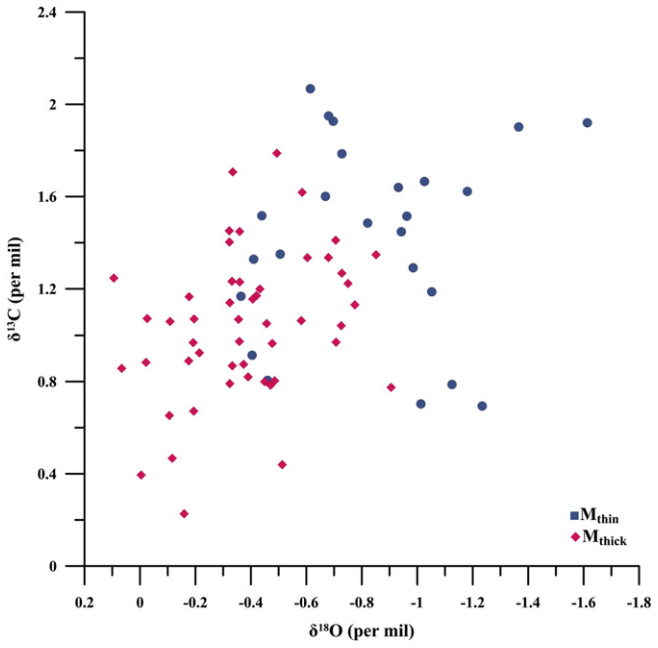

Fig. 9. M_{thin} and M_{thick} stable isotopic compositions displayed in $\delta^{18}O$ and $\delta^{13}C$ space.

In order to better understand how the combination of these effects influences the $\delta^{18}O$ compositions of our two morphotypes, we developed a conceptual model using depth profiles of the above mentioned parameters and average final chamber calcification depths for the two morphotypes for an upwelling (sample 21-8; Fig. 11a-d) and non-upwelling (sample 22-1; Fig. 11e-h) period. We use 25 and 35 m for M_{thin} and 55 and 100 m for M_{thick} for upwelling and non-upwelling periods, respectively (see Table 6 for parameter values and calculations

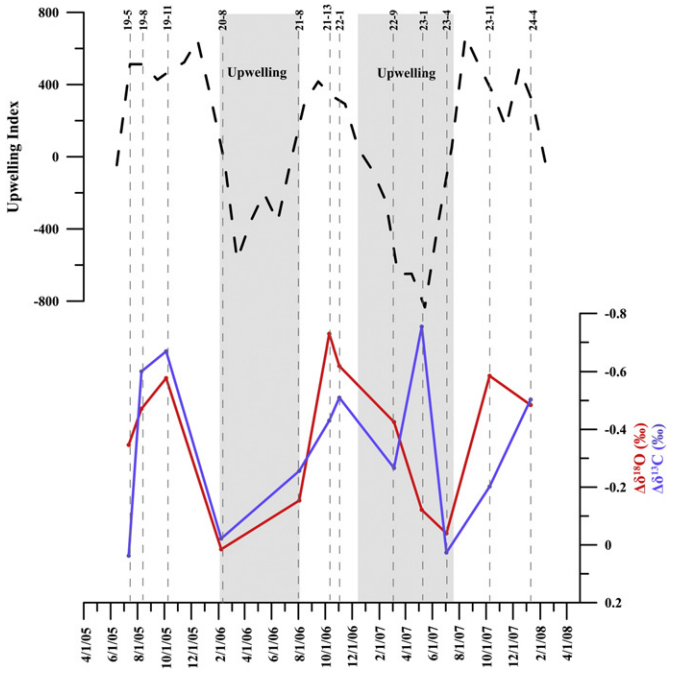

Fig. 10. The offset between M_{thin} and M_{thick} oxygen ($\Delta\delta^{18}O = M_{thin} - M_{thick}$; blue line) and carbon isotopic compositions ($\Delta\delta^{13}C = M_{thin} - M_{thick}$; pink line) and the averaged monthly upwelling index (black dashed line) with associated sample IDs.

Table 5
Sample depths and hydrographic data for M_{thin} and M_{thick}. Gray shaded regions indicate upwelling periods. All parameters are those collected at the estimated calcification depths.

Sample ID	Trap date	Hydro date	Date difference	$\delta^{13}C$ (‰)	$\delta^{18}O$ (‰)	$\delta^{18}O$ temp (°C)	Temperature (°C)	Temp difference (°C)	Depth (m)	Salinity	$[PO_4^{3-}]$ (μmol/kg)	Chl (ng/L)	O_2 (μmol/kg)	$[CO_3^{2-}]$ (μmol/kg)	pH	Sigma T (g/cm^3)	Irradiance[a] (μE m^{-2} s^{-1})
M_{thin}																	
19_5	7–13–2005	7–12–2005	–1	1.41	–0.71	23.4	23.1	0.3	45	36.9	0.24	418	152	181	7.99	25.3	
19_8	8–24–2005	8–10–2005	–14	1.42	–0.71	23.7	24.0	–0.3	15	37.0	0.04	215	181	202	8.02	25.1	
19_11	10–5–2005	10–5–2005	0	1.64	–0.76	23.4	23.4	0.0	88	36.9	0.28	169	147	195	7.98	25.2	
20_8	2–21–2006	2–7–2006	–14	1.14	–0.37	22.0	22.0	–0.1	35	36.8	0.35	834	139	169	7.95	25.6	10
21_3	6–14–2006	6–6–2006	–8														
21_8	8–23–2006	8–3–2006	–20	1.31	–0.65	23.0	22.5	0.5	15	36.9	0.00	757	178	198	8.01	25.5	218
21_13	11–1–2006	10–10–2006	–22	1.51	–1.05	24.2	24.1	0.1	75	36.7	0.05	832	192	176	8.04	24.9	
22_1	11–8–2006	11–2–2006	–6	1.67	–1.03	24.6	24.2	0.4	88	36.7	0.25	93	154	204	8.00	24.9	
22_9	2–28–2007	3–6–2007	6	1.46	–0.59	22.8	23.0	–0.2	7	36.7	0.03	801	206	225	8.02	25.2	514
23_1	5–16–2007	5–8–2007	–8	1.95	–0.68	23.5	24.0	–0.5	18	36.9	0.12	250	164	208	8.01	25.1	454
23_4	6–27–2007	7–3–2007	6	0.80	–0.46	22.2	22.2	0.0	45	36.8	0.41	217	129	161	7.93	25.5	21
23_11	10–3–2007	10–9–2007	6	1.28	–1.05	23.5	23.1	0.5	100	36.7	0.38	60	103	181	7.96	25.2	
24_4	1–8–2008	1–10–2008	2	1.50	–0.87	23.5	23.5	0.0	45	36.8	0.30	366	146	190	7.97	25.1	
Mean			–6	1.43	–0.74	23.3	23.3	0.0	47.92	36.8	0.20	418	158	191	7.99	25.2	243.45
1σ				0.29	0.22	0.8	0.8	0.3	32.35	0.1	0.15	304	28	18	0.03	0.2	235.71
M_{thick}																	
19_5	7–13–2005	7–12–2005	–1	1.45	–0.36	21.7	21.8	–0.1	88	36.9	0.40	103	135	154	7.94	25.7	
19_8	8–24–2005	8–10–2005	–14	0.82	–0.24	21.4	21.2	0.2	55	36.8	0.40	124	139	169	7.95	25.9	
19_11	10–5–2005	10–5–2005	0	0.97	–0.18	20.6	20.8	–0.2	130	36.8	0.45		124	158	7.92	25.9	
20_8	2–21–2006	2–7–2006	–14	1.12	–0.38	22.0	22.0	0.0	35	36.8	0.35	834	139	169	7.95	25.6	10
21_3	6–14–2006	6–6–2006	–8	1.19	–0.54	22.7	22.8	–0.1	35	36.9	0.13	221	141	182	7.97	25.4	
21_8	8–23–2006	8–3–2006	–20	1.05	–0.49	22.3	22.5	–0.2	15	36.9	0.00	757	178	169	8.01	25.5	218
21_13	11–1–2006	10–10–2006	–22	1.08	–0.32	20.7	20.5	0.3	115	36.7	0.56		124	148	7.89	25.9	
22_1	11–8–2006	11–2–2006	–6	1.16	–0.41	21.7	21.9	–0.2	115	36.7	0.43		133	170	7.94	25.6	
22_9	2–28–2007	3–6–2007	6	1.19	–0.16	20.8	20.8	0.0	55	36.7	0.50	104	126	159	7.91	25.8	7
23_1	5–16–2007	5–8–2007	–8	1.20	–0.56	22.9	22.7	0.2	25	36.9	0.15	250	153	186	7.97	25.5	240
23_4	6–27–2007	7–3–2007	6	0.83	–0.42	22.0	22.2	–0.2	45	36.8	0.41	217	129	161	7.93	25.5	21
23_11	10–3–2007	10–9–2007	6	1.08	–0.46	20.7	20.1	0.6	130	36.7	0.75		103	134	7.85	26.0	
24_4	1–8–2008	1–10–2008	2	1.00	–0.39	21.2	21.4	–0.2	75	36.7	0.50	135	125	153	7.91	25.7	
Mean			–6	1.09	–0.38	21.6	21.6	0.0	70.58	36.8	0.39	305	135	162	7.93	25.7	99.25
1σ				0.16	0.13	0.8	0.9	0.3	40.98	0.1	0.20	284	18	14	0.04	0.2	118.71

[a]Irradiance at estimated depth of calcification.

and Fig. 11 for depth profiles). In the model, we use Eqs. 4 and 5 to determine the expected $\delta^{18}O_{calcite}$ at the average depths of final chamber calcification for each morphotype during upwelling and non-upwelling periods (Table 5). In doing so, we were able show that modeled $\delta^{18}O_{calcite}$ offsets between the two morphotypes are minimal during periods of upwelling ($\delta^{18}O_{calcite}$ M_{thin} − M_{thick} = −0.05‰) and maximal during periods of non-upwelling ($\delta^{18}O_{calcite}$ M_{thin} − M_{thick} = −0.55‰). This is mostly attributed to changes in in-situ temperature at the respective calcification depths of the two morphotypes. The effect of irradiance on the $\delta^{18}O$ of foraminifera is negligible for the measured irradiance values at their respective calcification depths (1–54 μE m^{-2} s^{-1}; Spero, 1992). However, increases in $[CO_3^{2-}]$ can result in a decrease in $\delta^{18}O$ as illustrated in Spero et al. (1997):

$$\delta^{18}O = 1.56 - 0.002\left[CO_3^{2-}\right]. \quad (6)$$

Thus, the $[CO_3^{2-}]$ effect contributes an additional $\delta^{18}O_{calcite}$ M_{thin} − M_{thick} offset of −0.02 and −0.07‰ based on the calculated in-situ $[CO_3^{2-}]$ of the two morphotypes for upwelling and non-upwelling periods, respectively. The modeled total $\delta^{18}O_{calcite}$ M_{thin} − M_{thick} offset for upwelling (−0.07‰) and non-upwelling periods (−0.62‰) are comparable to the average offsets observed throughout the study period (−0.15‰ for upwelling and −0.54‰ for non-upwelling periods). Thus, the offsets in $\delta^{18}O$ between the two morphotypes can be explained by a combined difference in final chamber calcification depth and the associated differences in in-situ temperature and $[CO_3^{2-}]$.

The same principles can be applied to explain the $\delta^{13}C$ differences exhibited by M_{thin} and M_{thick} using upwelling/non-upwelling $\delta^{13}C_{DIC}$ profiles that are derived using the $\delta^{13}C_{DIC}$–$[PO_4^{3-}]$ relationship from Ortiz et al. (2000):

$$\delta^{13}C_{DIC} = -0.96\left[PO_4^{3-}\right] + 1.7. \quad (7)$$

We caution that this equation was derived for the California Current system and may not be ideal for the Cariaco Basin, but it is applicable for the purpose of this conceptual model. The $\delta^{13}C_{DIC}$ of the surface waters is high due to the preferential utilization of ^{12}C during photosynthesis and decreases with depth due to the remineralization of organic matter and release of ^{12}C (Fig. 11). Considering only changes in $\delta^{13}C_{DIC}$ with depth, we estimate a predicted $\delta^{13}C_{calcite}$ M_{thin} − M_{thick} offset of 0.13

Table 6
Conceptual model for carbon and oxygen isotopic differences in the Cariaco Basin *Orbulina unviersa* morphotypes.

$\delta^{18}O$ (‰)		Upwelling (21-8)	Non-upwelling (22-1)	N-U difference	$\delta^{13}C$ (‰)		Upwelling (21-8)	Non-upwelling (22-1)	N-U difference
	M_{thin} depth (m)	25	55			M_{thin} depth (m)	25	55	
	M_{thick} depth (m)	35	100			M_{thick} depth (m)	35	100	
	Temperature C					**$[PO_4^{3-}]$ (µmol/kg)**			
	M_{thin} Temperature	21.84	25.61			M_{thin} $[PO_4^{3-}]$ (µmol/kg)	0.20	0.13	
	M_{thick} Temperature	21.57	23.34			M_{thin} $[PO_4^{3-}]$ (µmol/kg)	0.33	0.31	
	Offset ($M_{thin-Mthick}$)	0.27	2.27			Offset ($M_{thin-Mthick}$)	-0.13	-0.18	
	Salinity					**Predicted $\delta^{13}C$ DIC (‰)[d]**			
	M_{thin} salinity	36.83	36.57			M_{thin} predicted $\delta^{13}C$ (‰)	1.51	1.58	
	M_{thick} salinity	36.82	36.79			M_{thick} predicted $\delta^{13}C$ (‰)	1.38	1.40	
	Offset ($M_{thin-Mthick}$)	0.02	-0.22			Offset ($M_{thin-Mthick}$ ‰)	0.13	0.17	
	Predicted $\delta^{18}O$ water (‰)[a]					**Predicted $\delta^{13}C$ calcite (‰)[e]**			
	M_{thin} predicted $\delta^{18}O_w$ (‰)	1.02	0.94			M_{thin} predicted $\delta^{13}C$ (‰)	1.51	1.58	
	M_{thick} predicted $\delta^{18}O_w$ (‰)	1.02	1.01			M_{thick} predicted $\delta^{13}C$ (‰)	1.38	1.40	
	Offset ($M_{thin-Mthick}$)	0.01	-0.07		I	Offset ($M_{thin-Mthick}$ ‰)	0.13	0.17	0.04
	Predicted $\delta^{18}O$ calcite (‰)[b]					**$[CO_3^{2-}]$ (µmol/kg)**			
	M_{thin} predicted $\delta^{18}O$ (‰)	-0.36	-1.23			M_{thin} $[CO_3^{2-}]$ (µmol/kg)	169	227	
	M_{thick} predicted $\delta^{18}O$ (‰)	-0.31	-0.69			M_{thick} $[CO_3^{2-}]$ (µmol/kg)	160	190	
I	Offset ($M_{thin-Mthick}$)	-0.05	-0.55	-0.50		Offset ($M_{thin-Mthick}$; µmol/kg)	8	37	
	$[CO_3^{2-}]$ (µmol/kg)					**Predicted $\delta^{13}C$ calcite (‰)[f]**			
	M_{thin} $[CO_3^{2-}]$ (µmol/kg)	169	227			M_{thin} predicted $\delta^{13}C$ (‰)	2.55	2.20	
	M_{thick} $[CO_3^{2-}]$ (µmol/kg)	160	190			M_{thick} predicted $\delta^{13}C$ (‰)	2.60	2.42	
	Offset ($M_{thin-Mthick}$)	8	37		II	Offset ($M_{thin-Mthick}$ ‰)	-0.05	-0.22	-0.17
	Predicted $\delta^{18}O$ calcite (‰)[c]					**Irradiance (µE m^{-2} s^{-1})**			
	M_{thin} predicted $\delta^{18}O$ (‰)	1.22	1.11			M_{thin} Irradiance (µE m^{-2} s^{-1})	54	20	
	M_{thick} predicted $\delta^{18}O$ (‰)	1.24	1.18			M_{thick} Irradiance (µE m^{-2} s^{-1})	21	1	
II	Offset ($M_{thin-Mthick}$)	-0.02	-0.07	-0.06		Offset ($M_{thin-Mthick}$)	33	19	
						Predicted $\delta^{13}C$ calcite (‰)[g]			
						M_{thin} predicted $\delta^{13}C$ (‰)	2.29	2.06	
						M_{thick} predicted $\delta^{13}C$ (‰)	2.07	1.54	
					III	Offset ($M_{thin-Mthick}$ ‰)	0.22	0.52	0.31
	$\delta^{18}O$ (‰) Offset ($M_{thin-Mthick}$ ‰)					**$\delta^{13}C$ (‰) Offset ($M_{thin-Mthick}$ ‰)**			
I + II	Modeled offset (M_{thin}-M_{thick} ‰)	-0.07	-0.62	-0.55	I + II + III	Modeled offset (M_{thin}-M_{thick} ‰)	0.30	0.47	0.18
	Measured offset (M_{thin}-M_{thick} ‰)	-0.15	-0.54	-0.40		Observed offset (M_{thin}-M_{thick} ‰)	0.25	0.41	0.16

[a] Eq. (5) (McConnell et al., 2009).
[b] Eq. (4) (Bemis et al., 1998, LL equation).
[c] Eq. (6) (Spero et al., 1997, LL equation).
[d] Eq. (7) (Ortiz et al., 2000).
[e] For *O. universa*, $\delta^{13}C^{DIC} = \delta^{13}C^{calcite}$ (Spero, 1992).
[f] Eq. (9) (Spero et al., 1997, LL equation).
[g] Eq. (8) (Spero and Williams, 1988).

and 0.17‰ for upwelling and non-upwelling periods, respectively. We also consider the combined effects of light intensity and $[CO_3^{2-}]$ on the predicted $\delta^{13}C$ and $\delta^{18}O$ offsets for the two morphotypes. Foraminiferal $\delta^{13}C$ is more sensitive to changes in light intensity and $[CO_3^{2-}]$ than $\delta^{18}O$, with increases in $\delta^{13}C$ as great as 1.1 to 1.8‰ for HL relative to LL conditions and a decrease in $\delta^{13}C$ of 0.42‰ for a 60 µmol/kg increase in $[CO_3^{2-}]$ (Spero and Williams, 1988, 1989; Lea et al., 1995; Spero et al., 1997). The irradiance effect is attributed to the preferential uptake of ^{12}C by the symbionts during photosynthesis, producing a ^{13}C-enriched microenvironment for foraminiferal calcification (Spero and De Niro, 1987). For the upwelling scenario (Fig. 11a-d), the irradiance values at 25 and 35 m are 54 and 21 µE m^{-2} s^{-1}, respectively. For the non-upwelling scenario, the irradiance values at 55 and 100 m are 20 and 1.25 µE m^{-2} s^{-1}, respectively. This would contribute an additional $\delta^{13}C$ offset of 0.22 and 0.52‰ between M_{thin} and M_{thick} for upwelling and non-upwelling periods, respectively, based on the culture calibrations of Spero and Williams (1988):

$$\delta^{13}C = 1.50 \times I^{0.106}. \quad (8)$$

The carbonate ion effect would result in an additional −0.05 and −0.22‰ offset in $\delta^{13}C$ values for M_{thin} relative M_{thick} for upwelling

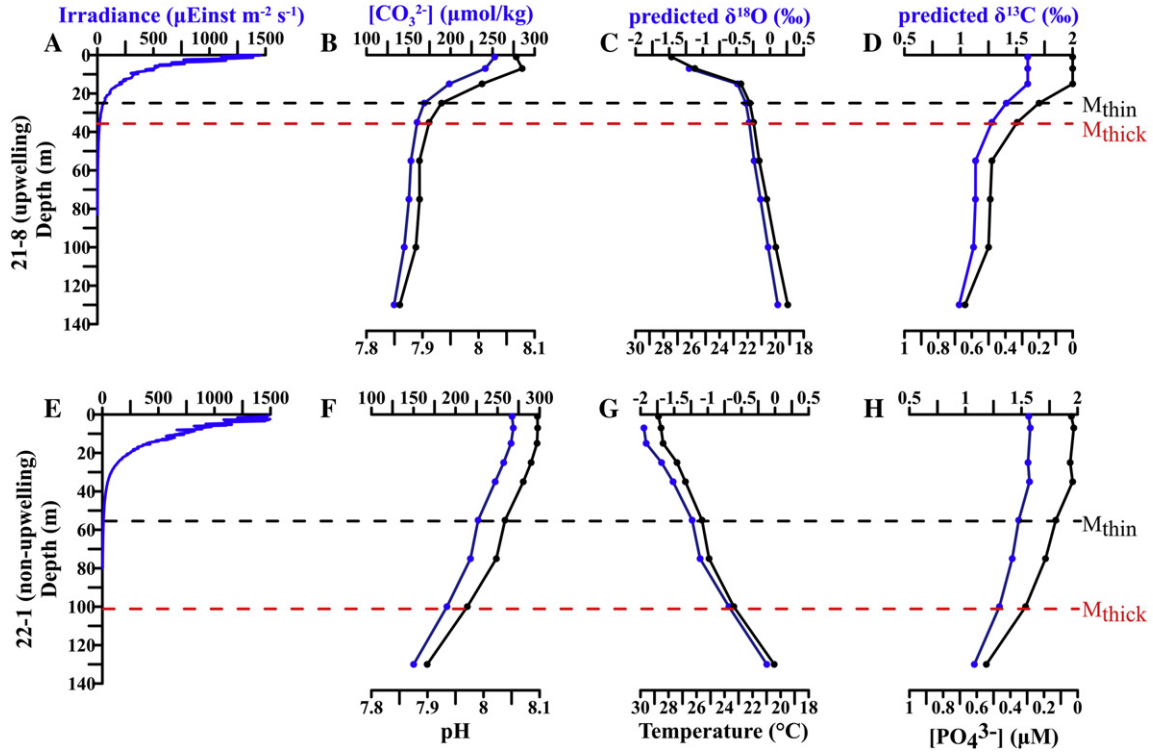

Fig. 11. Irradiance, $[CO_3^{2-}]$, pH, temperature, predicted $\delta^{18}O$, $[PO_4^{3-}]$, and predicted $\delta^{13}C$ depth profiles for upwelling sample 21-8 (A–D) and non-upwelling sample 22-1 (E–H). Black and red dashed lines mark the average calcification depths of M_{thin} and M_{thick}, respectively. .

and non-upwelling periods, respectively, based on the culture calibration of Spero et al., 1997:

$$\delta^{13}C = 3.56 - 0.006\left[CO_3^{2-}\right]. \quad (9)$$

As these effects have an opposing influence on $\delta^{13}C_{calcite}$, the $[CO_3^{2-}]$ effect mutes the strong influence of the irradiance effect on $\delta^{13}C_{calcite}$. Thus, the model predicts a total $\delta^{13}C_{calcite}$ M_{thin} − M_{thick} offset of 0.30 and 0.47‰ for upwelling and non-upwelling periods, respectively, due to the combined influence of $\delta^{13}C_{DIC}$, irradiance and $[CO_3^{2-}]$. These predicted offsets are comparable to the average observed offsets throughout the study period of 0.25 and 0.41‰ for upwelling and non-upwelling periods, respectively. Thus, elevated $\delta^{13}C$ in the shallower-dwelling M_{thin} relative to the deeper-dwelling M_{thick}, particularly during non-upwelling periods, may be due in large part to elevated symbiont photosynthesis during periods when M_{thin} is calcifying at higher light levels than M_{thick}, with additional contributions due to differences in in-situ $\delta^{13}C_{DIC}$ and $[CO_3^{2-}]$.

Another possible explanation for the stable isotopic differences between the two *O. universa* morphotypes is a difference in vital effects, assuming that the two morphotypes represent the Caribbean and Mediterranean cryptic species of *O. universa*. Vital effects is a term used to collectively describe differences in the geochemical compositions between species due to life processes such as respiration and symbiont photosynthesis (Spero et al., 1991; Zeebe, 1999). Just as there is a need to establish species-specific equations for various climate proxies (Wefer and Berger, 1991; Spero, 1998), it is likely that species-specific calibrations based on revised genetic taxonomies will be required as cryptic species continue to be identified. A preliminary study was conducted using cultured *O. universa* specimens collected from Catalina Island, California and Puerto Rico (H. Spero, unpub. obs.). This study collected juvenile *O. universa* from the upper 3–5 m of the water column in both locations and cultured the foraminifera at temperatures ranging from 9–29 °C. Only a single cryptic species of *O. universa* has been identified in the California Current System (Mediterranean (Type III; Kucera and Darling, 2002)) and the Caribbean cryptic species (Type I) has been identified in Puerto Rico (de Vargas et al., 1999). The results reveal that no systematic offset in the $\delta^{18}O$–temperature relationship exists between the *O. universa* specimens collected off Puerto Rico and Catalina Island. Though no genetic testing was performed to verify the genotypes of the cultured *O. universa*, this study suggests that there is no difference in oxygen isotopic composition of the cultured *O. universa* from the two different regions. Thus, the most likely explanation for the isotopic difference exhibited by the two morphotypes in the present study is that they differ in the average depths at which they calcify their final spherical chambers, as discussed earlier in this section.

4.3. Paleoceanographic implications and applications

As previously mentioned, the estimated final chamber calcification depths for the two morphotypes identified in this study are characterized by an ~2 °C temperature difference. This difference represents approximately half of the sea surface temperature change from the Last Glacial Maximum to the Holocene in the Caribbean (Schmidt et al., 2004; Foster, 2008). Because the isotopic offsets between the two morphotypes vary with the degree of surface ocean stratification, these differences may be muted in regions defined by a deep surface mixed layer. Conversely, larger isotopic offsets may exist between depth-stratified *O. universa* morphotypes/cryptic species in regions defined by a more stratified surface ocean. The observed stable isotopic differences between the two *O. universa* morphotypes could prove to be useful as a proxy for past changes in surface ocean stratification. Thus, future studies could utilize the stable isotopic offsets between *O. universa* morphotoypes in a given region as a method for reconstructing changes in upwelling intensity over various timescales.

In summary, the results of this study provide evidence that morphotypes of *O. universa*, though similar in their basic phenotypic expression, differ in their geochemical makeup and preferred calcification environments. Thus, it is important to distinguish between

them in order to eliminate scatter in paleoceanographic/paleoclimatic reconstructions.

5. Conclusions

Using a non-destructive morphometric method, we identify two distinct morphotypes of *O. universa* collected from sediment trap samples in the Cariaco Basin, Venezuela. We are unable to definitively assign each morphotype to a previously defined genotype (de Vargas et al., 1999) due to the use of formalin solution to preserve the sediment trap samples. However, using porosity and thickness measurements, as well as previously established ecological preferences (de Vargas et al., 1999; Morard et al., 2009), we conclude that the two morphotypes identified in this study represent the Caribbean and Mediterranean cryptic species of *O. universa*. The use of the non-destructive area density (ρ_A) method for identifying *O. universa* morphotypes allows for the subsequent isotopic analysis of foraminiferal samples. We find that the thin *O. universa* morphotype is defined by 0.34‰ higher and 0.38‰ lower average $\delta^{13}C$ and $\delta^{18}O$ values, respectively, than the thick morphotype, suggesting that they calcify their final chambers at different depths within the water column. The average estimated final chamber calcification depth offset of ~20 m results in an average calcification temperature offset of ~2 °C. The absolute offsets between *O. universa* morphotype $\delta^{13}C$ and $\delta^{18}O$ values increase/decrease during periods of non-upwelling/upwelling in the Cariaco Basin due to changes in the depth gradients of temperature, $\delta^{13}C_{DIC}$, irradiance and $[CO_3^{2-}]$. The relationship between the magnitude of morphotype $\delta^{13}C$ and $\delta^{18}O$ offset and surface ocean stratification suggests that the isotopic offsets between morphotypes may vary regionally depending on the depth of the mixed layer. These data provide evidence that *O. universa* morphotypes differ in their calcification environment and that the lumping of these morphotypes for geochemical analysis should be avoided as it may cause a significant amount of scatter in paleoreconstructions. The isotopic difference between the two morphotypes of *O. universa* could potentially be used as a proxy for reconstructing changes in surface ocean stratification. We recommend further research involving the genetic and subsequent geochemical analysis of *O. universa* collected from depth-stratified plankton tow samples to further explore the presence and geochemical differences among *O. universa* cryptic species in the world's oceans.

Supplementary data to this article can be found online at http://dx.doi.org/10.1016/j.marmicro.2015.08.001.

Acknowledgments

We thank Eric Tappa for his analytical contributions, particularly with the collection of sediment trap samples and stable isotopic measurements. We thank the Fundación La Salle de Ciencias Naturales, Estación de Investigaciones Marinas Isla Margarita (EDIMAR) and the crew of the *R/V Hermano Ginés* for their hard work at maintaining the CARIACO Time Series. We thank Pincelli Hull of Yale University and Jay Pickney of University of South Carolina for their advice on concept and statistical assessment. This research was supported by NSF award 1258991.

References

Astor, Y., Lorenzoni, L., Thunell, R., Varela, R., Muller-Karger, F., Troccoli, L., Taylor, G., Scranton, M., Tappa, E., Rueda, D., 2013. Interannual variability in sea surface temperature and fCO_2 changes in the Cariaco Basin. Deep-Sea Res. II 93, 33–43.

Aurahs, R., Treis, Y., Darling, K., Kucera, M., 2011. A revised taxonomic and phylogenetic concept for the planktonic foraminifer species *Globigerinoides ruber* based on molecular and morphometric evidence. Mar. Micropaleontol. 79, 1–14. http://dx.doi.org/10.1016/j.marmicro.2010.12.001.

Barker, S., Elderfield, H., 2002. Foraminiferal calcification response to glacial–interglacial changes in atmospheric CO_2. Science 297, 833–836. http://dx.doi.org/10.1126/science.1072815.

Bé, A.W.H., 1959. A method for rapid sorting of foraminifera from marine plankton samples. J. Paleontol. 33, 846–848.

Bé, A.W.H., Harrison, S.M., Lott, L., 1973. *Orbulina universa* d'Orbigny in the Indian Ocean. Micropaleontology 19, 150–192.

Bé, A.W.H., Hemleben, C., Anderson, O.R., Spindler, M., 1980. Pore structures in planktonic foraminifera. J. Foraminifer. Res. 10, 117–128.

Bé, A.W.H., Anderson, O.R., Caron, D.A., 1983. Sequence of morphological and cytoplasmic changes during gametogenesis in the planktonic foraminifer *Globigerinoides sacculifer* (Brady). Micropaleontology 29, 1–5.

Bemis, B.E., Spero, H.J., Bijma, J., Lea, D.W., 1998. Reevaluation of the oxygen isotopic composition of planktonic foraminifera: experimental results and revised paleotemperature equations. Paleoceanography 13 (2), 150–160.

Bemis, B.E., Spero, H.J., Thunell, R.C., 2002. Using species-specific paleotemperature equations with foraminifera: a case study in the Southern California Bight. Mar. Micropaleontol. 46, 405–430.

Bijma, J., Hemleben, C., Huber, B.T., Erlenkeuser, H., Kroon, D., 1998. Experimental determination of the ontogenetic stable isotope variability in two morphotypes of *Globigerinella siphonifera* d'Orbigny). Mar. Micropaleontol. 35, 141–160.

Billups, K., Spero, H.J., 1995. Relationship between shell size, thickness and stable isotopes in individual planktonic foraminifera from two equatorial Atlantic cores. J. Foraminifer. Res. 25 (1), 24–37. http://dx.doi.org/10.2113/gsjfr.25.1.24.

Bouvier-Soumagnac, Y., Duplessy, J.C., 1985. Carbon and oxygen isotopic composition of planktonic foraminifera from laboratory cultures, plankton tows, and recent sediments: implications for the reconstruction of paleoclimatic conditions and the global carbon cycle. J. Foraminifer. Res. 15, 302–320.

Bradshaw, J.S., 1959. Ecology of living planktonic foraminifera in the North and equatorial Pacific Ocean. Cushman Found. Foram. Res. Contrib. 10, 25–64.

Caron, D.A., Faber Jr., W.W., Bé, A.W.H., 1987. Growth of the spinose planktonic foraminifer *Orbulina universa* in laboratory culture and the effect of temperature on life processes. J. Mar. Biol. Assoc. U. K. 67, 343–358.

Colombo, M.R., Cita, M.B., 1980. Changes in size and test porosity of *Orbulina universa* d'Orbigny in the Pleistocene record of Cape Bojador (DSDP Site 397, Eastern North Atlantic). Mar. Micropaleontol. 5, 13–29.

Darling, K.F., Wade, C.M., 2008. The genetic diversity of planktic foraminifera and the global distribution of ribosomal RNA genotypes. Mar. Micropaleontol. 67, 216–238. http://dx.doi.org/10.1016/j.marmicro.2008.01.009.

Darling, K.F., Kroon, D., Wade, C.M., Leigh Brown, A.J., 1996. Molecular phylogeny of the planktonic foraminifera. J. Foraminifer. Res. 26, 324–330.

Darling, K.F., Wade, C.M., Kroon, D., Leigh Brown, A.J., 1997. Planktonic foraminiferal molecular evolution and their polyphyletic origins from benthic taxa. Mar. Micropaleontol. 30, 251–266.

Darling, K.F., Wade, C.M., Kroon, D., Leigh Brown, A.J., Bijma, J., 1999. The diversity and distribution of modern planktonic foraminiferal small subunit ribosomal RNA genotypes and their potential as tracers of present and past ocean circulations. Paleoceanography 14, 3–12.

de Vargas, C., Zaninetti, L., Hilbrecht, H., Pawlowski, J., 1997. Phylogeny and rates of molecular evolution of planktonic foraminifera: SSU rDNA sequences compared to the fossil record. J. Mol. Evol. 45, 285–294.

de Vargas, C., Norris, R., Zaninetti, L., Gibb, S.W., Pawlowski, J., 1999. Molecular evidence of cryptic speciation in planktonic foraminifers and their relation to oceanic provinces. Proc. Natl. Acad. Sci. 96, 2864–2868.

de Vargas, C., Saez, A.G., Medlin, L., Thierstein, H.R., 2003. Super-species in the calcareous plankton. In: Thierstein, H.R., Young, J.R. (Eds.), Coccolithophores, From Molecular Processes to Global Impact. Springer, Berlin, pp. 271–298.

Deuser, W.G., 1987. Seasonal variations in isotopic composition and deep-water fluxes of the tests of perennially abundant planktonic foraminifera of the Sargasso Sea: results from sediment-trap collections and their paleoceanographic significance. J. Foraminifer. Res. 17 (1), 14–27.

Deuser, W.G., Ross, E.H., 1989. Seasonally abundant planktonic foraminifera of the Sargasso Sea: succession, deep-water fluxes, isotopic compositions, and paleoceanographic implications. J. Foraminifer. Res. 19 (4), 268–293.

Deuser, W.G., Ross, E.H., Hemleben, C., Spindler, M., 1981. Seasonal changes in species composition, numbers, mass, size, and isotopic composition of planktonic foraminifera settling into the deep Sargasso Sea. Palaeogeogr. Palaeoclimatol. Palaeoecol. 33, 103–127.

Elderfield, H., Vautravers, M., Cooper, M., 2002. The relationship between shell size and Mg/Ca, Sr/Ca, $\delta^{18}O$, and $\delta^{13}C$ of species of planktonic foraminifera: planktonic foraminifera. Geochem. Geophys. Geosyst. 3, 1–13. http://dx.doi.org/10.1029/2001GC000194.

Erez, J., 1978. Vital effect on stable-isotope composition seen in foraminifera and coral skeletons. Nature 273, 199–202.

Foster, G.L., 2008. Seawater pH, pCO_2 and $[CO_3^{2-}]$ variations in the Caribbean Sea over the last 130 kyr: a boron isotope and B/Ca study of planktic foraminifera. Earth Planet. Sci. Lett. 271, 254–266. http://dx.doi.org/10.1016/j.epsl.2008.04.015.

Friedrich, O., Schiebel, R., Wilson, P.A., Weldeab, S., Beer, C.J., Cooper, M.J., Fiebig, J., 2012. Influence of test size, water depth, and ecology on Mg/Ca, Sr/Ca, $\delta^{18}O$ and $\delta^{13}C$ in nine modern species of planktic foraminifers. Earth Planet. Sci. Lett. 319–320, 133–145. http://dx.doi.org/10.1016/j.epsl.2011.12.002.

Goni, M., Woodworth, M., Aceves, H., Thunell, R., Tappa, E., Black, D., Muller-Karger, F., Varela, R., 2004. Generation, transport and preservation of the alkenone based UK37 sea surface temperature index in the water column and sediments of the Cariaco Basin, Venezuela. Glob. Biogeochem. Cycles 18. http://dx.doi.org/10.1029/2003GB002132 (GB2001).

Hamilton, C.P., Spero, H.J., Bijma, J., Lea, D.W., 2008. Geochemical investigation of gametogenic calcite addition in the planktonic foraminifera *Orbulina universa*. Mar. Micropaleontol. 68, 256–267.

Healy-William, N., Ehrlich, R., Williams, D.F., 1985. Morphometric and stable isotopic evidence for subpopulations of *Globorotalia truncatulinoides*. J. Foraminifer. Res. 15, 242–243.

Hecht, A.D., Bé, A.W.H., Lott, L., 1976. Ecologic and paleoclimatic implications of morphologic variation of *Orbulina universa* in the Indian Ocean. Science 194, 422–424.
Hemleben, C., Bijma, J., 1994. Foraminiferal population dynamics and stable carbon isotopes. In: Zahn, R. (Ed.), Carbon Cycling in the Glacial Ocean: Constraints on the Ocean's Role in Global ChangeNATO ASI Series. Springer-Verlag, Berlin, pp. 145–166.
Hemleben, C., Spindler, M., Anderson, O.R., 1989. Modern Planktonic Foraminifera. Springer.
Huber, B.T., Bijma, J., Darling, K.F., 1997. Cryptic speciation in the living planktonic foraminifer *Globigerinella siphonifera* (d'Orbigny). Paleobiology 23, 33–62.
Kennett, J.P., 1976. Phenotypic variation in some Recent and late Cenozoic planktonic foraminifera. In: Hedley, R.H., Adams, C.D. (Eds.), Foraminifera, v. 2. Academic Press, London, pp. 111–169.
Knowlton, N., 1993. Sibling species in the sea. Annu. Rev. Ecol. Evol. Syst. 24, 189–216.
Kucera, M., Darling, K.F., 2002. Cryptic species of planktonic foraminifera: their effect on palaeoceanographic reconstructions. Philos. Trans. R. Soc. A Math. Phys. Eng. Sci. 360, 695–718. http://dx.doi.org/10.1098/rsta.2001.0962.
Kuroyanagi, A., Kawahata, H., 2004. Vertical distribution of living planktonic foraminifera in the seas around Japan. Mar. Micropaleontol. 53 (1–2), 173–196. http://dx.doi.org/10.1016/j.marmicro.2004.06.001.
Lea, D.W., Martin, P.A., Chan, D.A., Spero, H.J., 1995. Calcium uptake and calcification rate in the planktonic foraminifer *Orbulina universa*. J. Foraminifer. Res. 25 (1), 14–23.
Lea, D.W., Mashiotta, T.A., Spero, H.J., 1999. Controls on magnesium and strontium uptake in planktonic foraminifera determined by live culturing. Geochim. Cosmochim. Acta 63 (16), 2369–2379.
Lombard, F., Labeyrie, L., Michel, E., Spero, H.J., Lea, D.W., 2009. Modelling the temperature dependent growth rates of planktic foraminifera. Mar. Micropaleontol. 70, 1–7. http://dx.doi.org/10.1016/j.marmicro.2008.09.004.
Lombard, F., da Rocha, R.E., Bijma, J., Gattuso, J.-P., 2010. Effect of carbonate ion concentration and irradiance on calcification in planktonic foraminifera. Biogeosciences 7, 247–255. http://dx.doi.org/10.5194/bg-7-247-2010.
Lorenzoni, L., Hu, C., Varela, R., Arias, G., Guzman, L., Muller-Karger, F., 2011. Bio-optical characteristics of Cariaco Basin (Caribbean Sea) waters. Cont. Shelf Res. 31, 582–593.
Marshall, B.J., Thunell, R.C., Henehan, M.J., Astor, Y., Wejnert, K.E., 2013. Planktonic foraminiferal area density as a proxy for carbonate ion concentration: a calibration study using the Cariaco Basin Ocean time series: foraminiferal area density [CO_3^{2-}] proxy. Paleoceanography 28, 363–376. http://dx.doi.org/10.1002/palo.20034.
McConnell, M.C., Thunell, R.C., Lorenzoni, L., Astor, Y., Wright, J.D., Fairbanks, R., 2009. Seasonal variability in the salinity and oxygen isotopic composition of seawater from the Cariaco Basin, Venezuela: implications for paleosalinity reconstructions. Geochem. Geophys. Geosyst. 10. http://dx.doi.org/10.1029/2008GC002035.
Morard, R., Quillévéré, F., Escarguel, G., Ujiie, Y., de Garidel-Thoron, T., Norris, R.D., de Vargas, C., 2009. Morphological recognition of cryptic species in the planktonic foraminifer *Orbulina universa*. Mar. Micropaleontol. 71, 148–165. http://dx.doi.org/10.1016/j.marmicro.2009.03.001.
Morard, R., Quillévéré, F., Escarguel, G., de Garidel-Thoron, T., de Vargas, C., Kucera, M., 2013. Ecological modeling of the temperature dependence of cryptic species of planktonic Foraminifera in the Southern Hemisphere. Palaeogeogr. Palaeoclimatol. Palaeoecol. 391, 13–33. http://dx.doi.org/10.1016/j.palaeo.2013.05.011.
Muller-Karger, F., Varela, R., Thunell, R., Scranton, M., Bohrer, R., Gordon, T., Capelo, J., Astor, Y., Tappa, E., Ho, T.-Y., Walsh, J.J., 2001. The annual cycle of primary production in the Cariaco Basin: implications for vertical export of carbon along a continental margin. J. Geophys. Res. 106, 4527–4542.
Ortiz, J.D., Mix, A.C., Wheeler, P.A., Key, R.M., 2000. Anthropogenic CO_2 invasion into the northeast Pacific based on concurrent $\delta^{13}C_{DIC}$ and nutrient profiles from the California Current. Glob. Biogeochem. Cycles 14 (3), 917.
Pelletier, G., Lewis, E., Wallace, D., 2007. CO2sys_ver16.xls: A Calculator for the CO_2 System in Seawater for Microsoft Excel/VBA. Washington State Department of Ecology/Brookhaven National Laboratory, Olympia, WA/Upton, NY, USA.
Ren, H., Sigman, D.M., Thunell, R.C., Prokopenko, M.G., 2012. Nitrogen isotopic composition of planktonic foraminifera from the modern ocean and recent sediments. Limnol. Oceanogr. 57, 1011–1024. http://dx.doi.org/10.4319/lo.2012.57.4.1011.
Richey, J.N., Poore, R.Z., Flower, B.P., Hollander, D.J., 2012. Ecological controls on the shell geochemistry of pink and white *Globigerinoides ruber* in the northern Gulf of Mexico: implications for paleoceanographic reconstruction. Mar. Micropaleontol. 82–83, 28–37. http://dx.doi.org/10.1016/j.marmicro.2011.10.002.
Sanyal, A., Hemming, N.G., Broecker, W.S., Lea, D.W., Spero, H.J., Hanson, G.N., 1996. Oceanic pH control on the boron isotopic composition of foraminifera: evidence from culture experiments. Paleoceanography 11 (5), 513–517. http://dx.doi.org/10.1029/96PA01858.
Sautter, L.R., Thunell, R.C., 1991. Seasonal variability in the $\delta^{18}O$ and $\delta^{13}C$ of planktonic foraminifera from an upwelling environment: sediment trap results from the San Pedro Basin, Southern California Bight. Paleoceanography 6, 307–334. http://dx.doi.org/10.1029/91PA00385.
Schmidt, D.N., Renaud, S., Bollmann, J., Schiebel, R., Thierstein, H.R., 2004. Size distribution of Holocene planktic foraminifer assemblages: biogeography, ecology and adaptation. Mar. Micropaleontol. 50, 319–338. http://dx.doi.org/10.1016/S0377-8398(03)00098-7.
Spero, H.J., 1987. Symbiosis in the planktonic foraminifer, *Orbulina universa*, and the isolation of its symbiotic dinoflagellate, *Gymnodinium bdii* sp. nov. J. Phycol. 23, 307–317.
Spero, H.J., 1988. Ultrastructural examination of chamber morphogenesis and biomineralization in the planktonic foraminifer *Orbulina universa*. Mar. Biol. 99, 9–20.
Spero, H.J., 1992. Do planktonic foraminifera accurately record shift in the carbon isotopic composition of seawater ΣCO_2? Mar. Micropaleontol. 19, 275–285.
Spero, H.J., 1998. Life history and stable isotope geochemistry of planktonic foraminifera. In: Norris, R.D., Corfield, R.M. (Eds.), Isotope Paleobiology and Paleoecology; Paleontological Society Papers. 4, pp. 7–36.
Spero, H.J., De Niro, M.J., 1987. The influence of symbiont photosynthesis on the $\delta^{13}O$ and $\delta^{13}C$ values of planktonic foraminiferal calcite. Symbiosis 4, 213–228.
Spero, H.J., Parker, S.L., 1985. Photosynthesis in the symbiotic planktonic foraminifer *Orbulina universa*, and its potential contribution to oceanic primary productivity. J. Foraminifer. Res. 15, 273–281.
Spero, H.J., Williams, D.F., 1988. Extracting environmental information from planktonic foraminiferal $\delta^{13}C$ data. Nature 335, 717–719.
Spero, H.J., Williams, D.F., 1989. Opening the carbon isotope "vital effect" black box. 1. Seasonal temperatures in the euphotic zone. Paleoceanography 4 (6), 593–601.
Spero, H.J., Lerche, I., Williams, D.F., 1991. Opening the carbon isotope "vital effect" black box, 2. Quantitative model for interpreting foraminiferal carbon isotope data. Paleoceanography 6, 639–655.
Spero, H.J., Bijma, J., Lea, D.W., Bemis, B.E., 1997. Effect of seawater carbonate concentration on foraminiferal carbon and oxygen isotopes. Nature 390, 497–500.
Spero, H.J., Mielke, K.M., Kalve, E.M., Lea, D.W., Pak, D.K., 2003. Multispecies approach to reconstructing eastern equatorial Pacific thermocline hydrography during the past 360 kyr. Paleoceanography 18 (1), 1022. http://dx.doi.org/10.1029/2002PA000814.
Spero, H.J., Eggins, S.M., Russell, A.D., Vetter, L., Kilburn, M.R., Hönisch, B., 2015. Timing and mechanism for intratest Mg/Ca variability in a living planktic foraminifer. Earth Planet. Sci. Lett. 409, 32–42. http://dx.doi.org/10.1016/j.epsl.2014.10.030.
Steinke, S., Chiu, H.Y., Yu, P.S., Shen, C.C., Löwemark, L., Mii, H.S., Chen, M.T., 2005. Mg/Ca ratios of two *Globigerinoides ruber* (white) morphotypes: implications for reconstructing past tropical/subtropical surface water conditions: *G. ruber* (white) Mg/Ca ratios. Geochem. Geophys. Geosyst. 6 (11). http://dx.doi.org/10.1029/2005GC000926.
Stewart, I.A., Darling, K.F., Kroon, D., Wade, C.M., Troelstra, S.R., 2001. Genotypic variability on subarctic Atlantic planktic foraminifera. Mar. Micropaleontol. 43, 143–153.
Takahashi, K., Bé, A.W.H., 1984. Planktonic–foraminifera — factors controlling sinking speeds. Deep Sea Res. Part A 31, 1477–1500. http://dx.doi.org/10.1016/0198-0149(84)90083-9.
Tedesco, K., Thunell, R., 2003. Seasonal and interannual variations in planktonic foraminiferal flux and assemblage composition in the Cariaco Basin, Venezuela. J. Foraminifer. Res. 33, 192–210.
Tendal, O., 1990. Why are Foraminiferida foraminifers? In: Hemleben, C., Kaminski, M.A., Kuhnt, W., Scott, D.B. (Eds.), Paleocology, Biostratigraphy, Paleoceanography and Taxonomy of Agglutinated ForaminiferaNATO ASI Series C 327. Kluwer, Boston, pp. 13–18
Tolderlund, S., Bé, A.W.H., 1971. Seasonal distribution of planktonic foraminifera in the western North Atlantic. Micropaleontology 17, 297–329.
Turich, C., Schouten, H., Thunell, R., Varela, R., Astor, Y., Wakeham, S., 2013. Comparison of TEX86 and temperature proxies in sinking particles in the Cariaco Basin. Deep-Sea Res. 78, 115–133.
Wang, L., 2000. Isotopic signals in two morphotypes of *Globigerinoides ruber* (white) from the South China Sea: implications for monsoon climate change during the last glacial cycle. Palaeogeogr. Palaeoclimatol. Palaeoecol. 161, 381–394.
Wefer, G., Berger, W.H., 1991. Isotope paleontology: growth and composition of extant calcareous species. Mar. Geol. 100, 207–248.
Wejnert, K.E., Thunell, R.C., Astor, Y., 2013. Comparison of species-specific oxygen isotope paleotemperature equations: sensitivity analysis using planktonic foraminifera from the Cariaco Basin, Venezuela. Mar. Micropaleontol. 101, 76–88.
Wolf-Gladrow, D.A., Bijma, J., Zeebe, R.E., 1999. Model simulation of the carbonate chemistry in the microenvironment of symbiont bearing foraminifera. Mar. Chem. 64, 181–198. http://dx.doi.org/10.1016/S0304-4203(98)00074-7.
Zeebe, R.E., 1999. An explanation of the effect of seawater carbonate concentration on foraminiferal oxygen isotopes. Geochim. Cosmochim. Acta 63, 2001–2007.